Retrievals of soil moisture and vegetation optical depth using a multi-channel collaborative algorithm

Citation: Tianjie Zhao, Jiancheng Shi, Dara Entekhabi, Thomas J. Jackson, Lu Hu, Zhiqing Peng, Panpan Yao, Shangnan Li, Chuen Siang Kang, Retrievals of soil moisture and vegetation optical depth using a multi-channel collaborative algorithm, Remote Sensing of Environment, Volume 257, 2021

As Published: 10.1016/J.RSE.2021.112321

Publisher: Elsevier BV

Persistent URL: https://hdl.handle.net/1721.1/132967

Version: Final published version: final published article, as it appeared in a journal, conference proceedings, or other formally published context

Remote Sensing of Environment 257 (2021) 112321

Contents lists available at ScienceDirect

Remote Sensing of Environment

journal homepage: www.elsevier.com/locate/rse

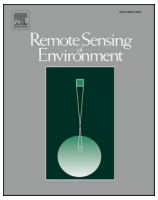

Retrievals of soil moisture and vegetation optical depth using a multi-channel collaborative algorithm

Tianjie Zhao [a], Jiancheng Shi [b,*], Dara Entekhabi [c], Thomas J. Jackson [d], Lu Hu [e], Zhiqing Peng [a,f], Panpan Yao [a], Shangnan Li [g], Chuen Siang Kang [h]

[a] State Key Laboratory of Remote Sensing Science, Aerospace Information Research Institute, Chinese Academy of Sciences, China
[b] National Space Science Center, Chinese Academy of Sciences, China
[c] Department of Civil and Environmental Engineering, Massachusetts Institute of Technology, United States
[d] USDA-ARS Hydrology and Remote Sensing Laboratory (Retired), United States
[e] International Institute for Earth System Science, Nanjing University, China
[f] University of Chinese Academy of Sciences, China
[g] Unit 93920, China
[h] Department of Geoinformation, Faculty of Built Environment & Surveying, Universiti Teknologi Malaysia, Malaysia

ARTICLE INFO

Keywords:
Soil moisture
Vegetation optical depth
Multi-channel
Multi-angular
Multi-frequency
Field experiment

ABSTRACT

Due to the success of the SMOS (Soil Moisture and Ocean Salinity) and SMAP (Soil Moisture Active Passive) missions, new satellite missions are on the horizon. The current and future missions can benefit from investigations that seek to improve retrieval algorithms that quantitatively map global soil moisture and vegetation optical depth (tau) from Earth's microwave emissions. In this study, we explore multi-angular and multi-frequency approaches for the retrieval of soil moisture and vegetation tau, considering the payload configurations of current and future satellite missions (such as the Copernicus Imaging Microwave Radiometer, the Water Cycle Observation Mission, and the Terrestrial Water Resources Satellite) using a new set of ground observations. Two ground-based microwave radiometry datasets collected in Inner Mongolia during the Soil Moisture Experiment in the Luan River from July to August 2017 (cropland) and August to September 2018 (grassland) are used for this study. The corn field, which covers an entire growth period, indicated that the degree of information increases linearly as the number of channels (in terms of the incidence angle and frequency) increases, and that the multi-frequency observations contain slightly more independent information than do the multi-angular observations under the same number of channels. The polarization difference in brightness temperature is sensitive to both soil moisture and vegetation water content, especially at L-band due to its penetrating ability. Soil moisture explains most of the variance in frequency differences of brightness temperature at adjacent frequencies (L- & C-bands, C- & X-bands), while the variance in incidence-angle differences of brightness temperature is mostly associated with the vegetation water content. A multi-channel collaborative algorithm (MCCA) is developed based on the two-component version of the omega-tau model, which utilizes information from collaborative channels expressed as an analytical form of brightness temperature at the core channel to rule out the parameters to be retrieved. Results of soil moisture retrieval show that the multi-angular approach used by the MCCA generally has a better performance, unbiased root mean square difference (ubRMSD) varying from 0.028 cm^3/cm^3 to 0.037 cm^3/cm^3, than the multi-frequency approach (ubRMSD from 0.028 cm^3/cm^3 to 0.089 cm^3/cm^3) for the corn field. This is attributed to the dependence of vegetation tau on the frequency being more significant than that on the incidence angle. Except for in the C- & X-band combination, the multi-frequency approach used by the MCCA performs better (ubRMSD from 0.018 cm^3/cm^3 to 0.023 cm^3/cm^3) than the multi-angular version (ubRMSD from 0.026 cm^3/cm^3 to 0.034 cm^3/cm^3) for the grass field due to reduced vegetation effects for this type of cover. It is affirmed that increasing the number of observation channels could make the soil moisture retrieval more robust, but might also limit the retrieval performance, as the probability that the model estimations will not match the observations is increased. This study provides new insights into the design of potential satellite missions to improve soil moisture retrieval. A satellite with simultaneous multi-angular and multi-frequency observation capabilities is highly recommended.

* Corresponding author at: National Space Science Center, Chinese Academy of Sciences, NO.1 Nanertiao, Zhongguancun, Haidian District, Beijing 100190, China.
E-mail address: shijiancheng@nssc.ac.cn (J. Shi).

https://doi.org/10.1016/j.rse.2021.112321
Received 7 May 2020; Received in revised form 26 January 2021; Accepted 28 January 2021
Available online 22 February 2021

1. Introduction

Soil moisture information is critically important in hydrological processes due to its relationships with land surface evapotranspiration, runoff, precipitation and infiltration (Vereecken et al., 2008; Seneviratne et al., 2010; Corradini, 2014; Brocca et al., 2017; Zhao et al., 2020a). Soil moisture (volumetric water content) at watershed scales can be measured using the direct gravimetric method and other indirect methods such as neutron attenuation, gamma absorption, and time/frequency domain reflectometry (Cosh et al., 2006; Robinson et al., 2008; Dorigo et al., 2011). Such information is crucial in a wide variety of processes and applications and has been playing a significant role in numerical weather predictions, flood forecasting, drought assessments and regional water resource management. However, these in situ measurements are insufficient to provide comprehensive information for a global perspective due to the differences in their measurement principles and spatial representations. Remote sensing, especially methods using microwave radiometry, has been investigated as technology for the global mapping of soil moisture since the Skylab mission in the 1970s (Jackson et al., 2004). Many efforts have been dedicated to exploring the remote sensing technologies and the methodology for soil moisture mapping at a global scale by a growing scientific community. It is now well known that the soil moisture contribution and vegetation effects in terms of absorption and scattering are coupled and that the vegetation optical depth (tau) is related to the vegetation water content, canopy structures, woody biomass (Rahmoune et al., 2014; Rodríguez-Fernández et al., 2018) and carbon stock (Brandt et al., 2018; Fan et al., 2019), which may support additional scientific applications.

The Advanced Microwave Scanning Radiometer for EOS (AMSR-E) is a twelve-channel, six-frequency (from 6.9 to 89 GHz) passive microwave radiometer (Kawanishi et al., 2003) with spatial resolutions ranging from 75 × 43 km (6.9 GHz) to 6 × 4 km (89 GHz). Although the C-band and X-band are not the optimal frequencies for the remote sensing of soil moisture, a number of efforts have been made to develop and validate retrieval algorithms. The NASA (National Aeronautics and Space Administration) algorithm for AMSR-E was originally developed as an iterative algorithm (Njoku and Li, 1999) that utilizes multi-frequency information (6.9, 10.6 and 18 GHz, dual-polarizations) to retrieve the soil moisture with a consistent vegetation tau value for all frequencies (Njoku et al., 2003). It was then replaced with a regression algorithm, in which the vegetation and roughness effects are considered to be similar and could be combined into one parameter to describe their exponential dependences, thus reducing the number of unknowns. Results of the combined effects of vegetation and roughness from AMSR-E showed frequency dependence and seasonal variability (Njoku and Chan, 2006). A similar iterative approach was developed by Paloscia et al. (2006) with initial tau values estimated from the polarization difference (PI) at X-band. The JAXA (Japan Aerospace Exploration Agency) selects an alternative method as the standard algorithm, which uses the index of soil moisture (ISW, brightness temperature difference between frequencies) and PI to perform the retrieval based on the look-up table method (Koike et al., 2004). The land parameter retrieval model (LPRM) utilizes the microwave polarization difference index (MPDI), which is analytically expressed as a function of soil moisture and vegetation tau (Meesters et al., 2005) by assuming that the vegetation signals are independent on polarization, to derive both soil moisture and vegetation tau (Owe et al., 2001; De Jeu and Owe, 2003). Aiming to separate the contributions of soil and vegetation, microwave vegetation indices (MVIs) were developed based on multi-frequency microwave observations from AMSR-E (Shi et al., 2008), and these indices were further utilized to derive vegetation transmissivity and then soil moisture (Zhao et al., 2011). Separately from the microwave-only algorithms mentioned above, vegetation tau can be obtained from ancillary optical vegetation indices; then, soil moisture can be retrieved based on a single-channel observation (Jackson, 1993; Jackson et al., 2010). The operation of the AMSR-E sensor with multi-frequency observations provided rich information across wavelengths but also brought challenges to the retrieval of parameters that vary with frequency. These challenges have promoted the development of various soil moisture algorithms that could be transferred to other satellite missions (Jackson, 1997; Jackson and Hsu, 2001; Owe et al., 2008; Dorigo et al., 2017) and generate a longer temporal record of soil moisture for climate change studies (Jung et al., 2010).

The Soil Moisture and Ocean Salinity (SMOS) mission provides unique multi-angular and full-polarization observations at L-band with a spatial resolution from 35 to 50 km depending on the incidence angle (Kerr et al., 2010). SMOS was launched in 2009 and has provided invaluable data for a variety of applications, including soil moisture mapping, vegetation property estimations and phenology analyses. The specialty of SMOS data (dual-polarization, multi-angular observations) was found to be suited to the 2-parameter (2-P) approach suggested by Wigneron et al., 1995a; the 2-P approach can be used to retrieve the soil moisture and vegetation biomass simultaneously at L-band (Wigneron et al., 2003). The official SMOS algorithm was developed based on the L-band Microwave Emission of the Biosphere (L-MEB) model (Wigneron et al., 2007) and has provided reliable retrievals of soil moisture (Jackson et al., 2012), vegetation tau and other related parameters through the iterative minimization of the cost function, which is the sum of the weighted squared differences between the simulated and observed brightness temperatures at multiple incidence angles (Kerr et al., 2012). Notably, the atmosphere effect is considered, and the vegetation temperature and soil temperature are different in the SMOS algorithm.

The continuous improvement of the SMOS algorithm has mainly focused on the refinement of brightness temperatures and introduction of multi-orbit observations, parameterizations and parameter optimizations of vegetation and roughness effects, the implementation of new soil dielectric models, etc. Angle-binned brightness temperatures in the ground reference frame were generated based on the SMOS snapshot-based dataset, and the soil moisture was retrieved based on multi-orbit observations for enhanced robustness (Al Bitar et al., 2017). In the original algorithm, the initial values of vegetation tau represent a combination of vegetation interception, vegetation laying under the canopy and standing vegetation (Wigneron et al., 2007; Kerr et al., 2012); thus, vegetation tau is considered to be a linear function of the leaf area index. It was later shown that at the global scale, different vegetation cover types require specific coefficients of the linear function, especially over densely vegetated zones (Rahmoune et al., 2013). The SMOS-IC (Institut National de la Recherche Agronomique and Centre d'Etudes Spatiales de la BIOsphère) algorithm (Fernandez-Moran et al., 2017a) chooses not to rely on auxiliary vegetation information as the initial input values but instead uses the yearly average values of vegetation tau from previous runs in the retrieval process. Additionally, new effective single scattering albedo values (Fernandez-Moran et al., 2017b) were derived based on the International Geosphere-Biosphere Programme (IGBP) land cover types (0.06 for forest regions, 0.06–0.12 for other regions). It was found that the newly derived vegetation tau is better correlated with the normalized difference vegetation index (NDVI) in most regions of the globe than the SMOS L3 products were. Soil surface roughness parameterization schemes (Peng et al., 2017) and their parameter settings are another important factor influencing the accuracy soil moisture retrievals. Numerous studies relating to the parameterization and calibration of surface roughness parameters for SMOS retrievals have been conducted (Lawrence et al., 2013; Zhao et al., 2015a; Wigneron et al., 2017). More recently, Fernandez-Moran et al. (2017b) showed that the roughness parameter varies in the range of 0.1–0.5, and constant values could be used at a global scale for SMOS-IC retrievals. In addition, Zhao et al. (2015b) refined the multi-angular behavior of the SMOS brightness temperature based on a two-step regression approach, and it was found that soil moisture and vegetation tau could be retrieved using the derivation form of the multi-angular MVIs (Cui et al., 2015; Cui et al., 2016). Another important finding is that the Mironov dielectric constant model (Mironov et al.,

2004) works well at both the dry end and the wet end and improves SMOS soil moisture retrievals (Mialon et al., 2015). The unique feature of multi-angular observations at L-band of SMOS makes it possible to retrieve soil moisture and vegetation tau values simultaneously, as it is more reasonable to assume the consistency of vegetation tau at varying incidence angles, and this feature significantly promotes the application of vegetation tau in above-ground carbon and land-atmosphere exchange studies.

The Soil Moisture Active Passive (SMAP) mission (Entekhabi et al., 2010) provides L-band brightness temperatures with multiple polarizations at a constant incidence angle of 40° with a spatial resolution of approximately 40 km. The development of SMAP radiometer-only soil moisture algorithms was based on the heritage leveraged from previous AMSR-E and SMOS missions. In the early release of SMAP soil moisture products (O'Neill et al., 2018), five optional algorithms were suggested, including the single-channel algorithm at horizontal polarization (SCA—H), single-channel algorithm at vertical polarization (SCA-V), dual-channel algorithm (DCA), extended dual-channel algorithm (EDCA), and LPRM. The SCA-H/V algorithms require vegetation tau inputs derived from a MODIS-based (moderate resolution imaging spectroradiometer) vegetation index climatology (Bindlish et al., 2011), and it was found that SCA-V delivered the best performance among algorithms over several core validation sites (Chan et al., 2016; Colliander et al., 2017). DCA and EDCA utilize different cost functions to combine dual-polarized observations to retrieve both soil moisture and vegetation tau. Theoretically, DCA and EDCA converge to the same solutions, and both algorithms rely on MODIS-derived vegetation tau values as constraints. The LPRM algorithm, as mentioned above, derives both soil moisture and vegetation tau using MPDI values as restrictions.

As SMAP only provides dual-polarization brightness temperatures for soil moisture retrieval, which are also correlated, Konings et al. (2016) introduced the multi-temporal dual-channel algorithm (MT-DCA) to enhance the robustness of retrievals. It is argued that vegetation tau values change more slowly than do soil moisture values, and vegetation tau can thus be assumed to be almost constant between every set of two consecutive overpasses. The MT-DCA adds an additional constraint to the retrieval by using a moving window of two consecutive overpasses at a given time of day and jointly retrieves a single vegetation tau value and two soil moisture values. In addition, the time series approach allows the retrieval of a single temporally constant value of the effective single scattering albedo (Konings et al., 2017). Chaubell et al. (2020) further showed that updates to the Wigneron-Lawrence roughness parameterization scheme (Wigneron et al., 2011; Lawrence et al., 2013) achieved improved accuracy and that SCA-V still outperformed all the implemented algorithms. The SMAP enhanced passive soil moisture was developed, and the assessment also affirmed that SCA-V delivered the best retrieval performance (Chan et al., 2018; O'Neill et al., 2019). On the other hand, Ebtehaj and Bras (2019) showed that the least-squares inversion of the omega-tau model is not strictly convex and that widely used, unconstrained, damped least-squares can lead to biased retrievals. Thus, they proposed a new constrained multi-channel algorithm (CMCA) that bounds the retrievals with a priori information about soil type and vegetation density, leading to high-resolution retrievals. To further reduce the uncertainty of soil moisture retrievals, Gao et al. (2020) designed the combined CMCA with a priori climatological constraints to improve both the spatial resolution and retrievals of vegetation tau. Although SMAP provides less independent information than the SMOS mission does, it was found that SMAP soil moisture retrievals, especially SCA-V retrievals, performed better than or comparably to SMOS retrievals (Al-Yaari et al., 2017; Chen et al., 2018; Al-Yaari et al., 2019), which indicates that more independent information may not improve the retrieval of soil moisture. Still, many issues with the radiative transfer equation (RTE) and retrieval algorithms remain to be resolved.

Selected papers regarding soil moisture retrieval algorithms are summarized in Table 1 and can be divided into three categories:

i. Algorithms based on the reverse-order RTE. These algorithms normally utilize the optimum radiometric channels and require ancillary information on vegetation, such as NDVI and leaf area index (LAI), to account for the vegetation contribution. The algorithm performance relies on a set of well-calibrated model parameters related to vegetation and roughness (Jackson, 1993; Zhao et al., 2014; Kang et al., 2020).
ii. Iterative algorithms based on forward simulations of RTE. Such algorithms fully utilize multiple information from different frequencies and angles through a cost function between forward simulations and observations. A priori information is often applied as constraints to avoid issues with multiple minima (Njoku et al., 2003; Kerr et al., 2012; Konings et al., 2017; Fernandez-Moran et al., 2017a; Chaubell et al., 2020; Gao et al., 2020).
iii. Algorithms based on microwave indices. These algorithms utilize unique information in a sophisticated way by combining data from different channels in appropriate indices, which maximize/minimize their relationship with certain geophysical variables (temperature, vegetation, roughness, soil moisture). Uncertainties in these algorithms mainly depend on the various assumptions introduced in the simplification of the radiative transfer processes (Owe et al., 2001; De Jeu and Owe, 2003; Koike et al., 2004; Paloscia et al., 2006; Njoku and Chan, 2006; Jones et al., 2009; Zhao et al., 2011; Shi et al., 2019).

Notably, various specific assumptions are involved in different soil moisture retrieval algorithms as shown in Table 1. Some commonly employed assumptions include ignoring atmospheric effects, setting the vegetation temperature equal to the soil temperature, applying polarization-independent vegetation parameters and time-stable or calibrated constant parameters such as the effective single scattering albedo and surface roughness parameters; the applicability of these assumptions must be investigated in the future to improve soil moisture retrievals. The foreseeable method for this investigation is to improve our understanding of the microwave radiative transfer process, especially inside vegetation, while continuing to increase the amount of independent information in terms of incidence angle, frequency, and polarization and reducing the number of assumptions to create better algorithms for more robust retrieval of more parameters.

With the success of SMOS and SMAP but aging mission, it is understood that continuous observations of soil moisture and vegetation properties from space are vital for a broad scientific community. SMOS-HR (high-resolution) aims to provide 10-km resolution observations at L-band with a multi-angular capability through 2-dimensional aperture synthesis (Rodriguez-Fernandez et al., 2019). The Copernicus Imaging Microwave Radiometer (CIMR) would carry an L-band radiometer that conically scans to obtain observations at a fixed incidence angle (55°) but with multi-frequency capabilities at L-band (< 60 km), C- and X-band (< 15 km), Ku-band (< 5.5 km) and Ka-band (< 5 km) (Kilic et al., 2018). China has been seeking new opportunities for soil moisture missions, including the Water Cycle Observation Mission (WCOM, 1-dimensional synthetic aperture radiometer at L-/S-/C-bands, Shi et al., 2014) and the Terrestrial Water Resources Satellite (TWRS, 1-dimensional synthetic aperture radiometer and radar at L-band, Zhao et al., 2020a). The spatial resolution of the WCOM is targeted in the range of 15 (C-band) to 50 km (L-band), while the TWRS would achieve a spatial resolution of approximately 18 km at L-band with a 12 × 10-m reflector antenna. The issue with a 1-dimensional radiometer is that the incidence angle varies across the satellite swath (Zhao et al., 2020b), but these two configurations could provide multi-frequency or active-passive observations, respectively. Despite the difficulties associated with hardware technology and the differences in their spatial resolutions, the objectives of this study are (i) which payload configuration may have the best performance in retrieving soil moisture and vegetation tau if we can only choose either a multi-frequency or multi-angle capability, and (ii) to

Table 1
Summary of selected soil moisture retrieval algorithms and their descriptions.

References	Algorithm/Model	Solution of RTE	Key approaches	Main assumptions
Jackson, 1993	Single-channel algorithm: SCA (SMAP baseline algorithm)	Reverse-order solution	To use ancillary data (land cover map, NDVI) for vegetation effects correction.	Thermal equilibrium; Constant vegetation (omega, b-parameter) and roughness parameters depending on land cover types.
Njoku and Li, 1999 Njoku et al., 2003	Multi-frequency algorithm	Iterative solution	To use multi-frequency (6.9, 10.6, and 18 GHz, V- and H-pol) information to iteratively derive soil moisture, vegetation water content and surface temperature values.	Thermal equilibrium; Vegetation parameters (omega, tau) are polarization-independent.
O'Neill et al., 2018 Chaubell et al., 2020	Dual-channel algorithm: DCA (SMAP option algorithm)	Iterative solution	To use dual-channel (V- and H-pol) information to iteratively derive soil moisture and vegetation tau values.	Thermal equilibrium; Vegetation parameters (omega, tau) are polarization-independent; Pixel-wise roughness parameter (non-time-varying).
Konings et al., 2016 Konings et al., 2017	Multi-temporal dual-channel algorithm: MT-DCA	Iterative solution	To use multi-temporal information (two adjacent overpasses) to enable the additional retrieval of effective omega values.	Thermal equilibrium; Vegetation parameters (omega, tau) are polarization-independent; Constant roughness parameter and non-time-varying omega.
Ebtehaj and Bras, 2019 Gao et al., 2020	Constrained multi-channel algorithm: CMCA	Iterative solution	To use priori information regarding soil type and vegetation to constrain least-square retrievals of soil moisture.	Thermal equilibrium; Vegetation parameters (omega, tau) are polarization-independent; Constant vegetation (omega, b-parameter) and roughness parameters depending on land cover types.
Owe et al., 2001 De Jeu and Owe, 2003	Land parameter retrieval model: LPRM	Traversal solution	To use an analytical form of vegetation tau expressed as a function of soil emissivity (moisture) and the MPDI.	Thermal equilibrium; Vegetation parameters (omega, tau) are polarization-independent.
Paloscia et al., 2001 Paloscia et al., 2006	Dual-frequency algorithm	Iterative solution	To use the PI at X-band for the estimation of initial vegetation tau values.	Thermal equilibrium; Vegetation parameters (omega, tau) are polarization-independent; Roughness effects are disregarded.
Koike et al., 2004 Fujii et al., 2009	Index of soil wetness algorithm (AMSR2 standard algorithm)	Look-up table	To use the ISW and PI (temperature independent) to simultaneously retrieve soil moisture and vegetation water content values, considering the fractional vegetation coverage.	Thermal equilibrium; Constant temperature, vegetation (omega, b-parameter) and roughness parameters at a global scale.
Njoku and Chan, 2006	Normalized polarization difference algorithm: NPD (AMSR-E standard algorithm)	Regression	To use the MPDI and the vegetation-roughness parameter to estimate soil moisture.	Thermal equilibrium; Vegetation parameters (omega = 0, tau) are polarization-independent.
Jones et al., 2009 Jones et al., 2011	Land surface retrieval algorithm	Iterative solution	To use the land-water emissivity slope index to derive vegetation tau values, considering the water fraction correction.	Thermal equilibrium; Vegetation parameters (omega, tau) are polarization-independent; Ignoring the soil surface reflection and its roughness effects (or incorporated with vegetation effects).
Wigneron et al., 1995a Fernandez-Moran et al., 2017a	2-Parameter algorithm (SMOS-IC algorithm)	Iterative solution	To use multi-angular information (V- and H-pol) to simultaneously retrieve soil moisture and vegetation tau, which is initially estimated from previous runs.	Constant vegetation (omega) and roughness parameters depending on land cover types; Vegetation (tau) is isotropic for V- and H-pol.
Kerr et al., 2012 Al Bitar et al., 2017	Multi-angular algorithm (SMOS standard algorithm)	Iterative solution	To use multi-angular information (V- and H-pol) to simultaneously retrieve soil moisture and vegetation tau, considering the angular antenna pattern and pixel heterogeneity.	Different vegetation (omega) and roughness parameters for either low vegetation and forest regions; Vegetation (tau) is isotropic for V- and H-pol.
Zhao et al., 2011 Shi et al., 2019	Multi-channel collaborative algorithm	Analytical solution	To use the MVIs to analytically derive vegetation transmissivity.	Thermal equilibrium; Vegetation parameters (omega = 0, tau) are polarization-independent.
This study	Multi-channel collaborative algorithm	Traversal/ Iterative solution	To use an analytical form of brightness temperatures at any two channels (polarization, incidence angle and frequency) as conditional restrictions.	The functional relationship between vegetation tau at different channels (polarization, incidence angle and frequency)

V-pol: vertical polarization; H-pol: horizontal polarization; RTE: radiative transfer eq.; NDVI: normalized difference vegetation index; MPDI: microwave polarization difference index; PI: polarization difference; ISW: index of soil wetness; MVIs: microwave vegetation indices; Omega: single scattering albedo; Tau: optical depth; b-parameter: vegetation optical depth coefficient

design a general retrieval algorithm that could fully utilize multi-channel information based on our current understanding of radiative transfer processes.

In this study, we aimed to explore the independent information contained within multi-angular and multi-frequency microwave observations and their sensitivities to soil moisture with new experimental data obtained during the Soil Moisture Experiment in the Luan River (SMELR), as described in Section II. The methodologies are presented in Section III, and a new retrieval algorithm was developed with which to examine the performances in retrieving soil moisture and vegetation tau through multi-frequency and multi-angular observation strategy configurations. The results and discussion in Section IV are expected to provide a reference for the development of future satellite missions for global soil moisture mapping.

2. Experimental data

The experimental data are ground-based measurements obtained from the Soil Moisture Experiment in the Luan River (SMELR, Zhao et al., 2020a), including observations of croplands in 2017 and grasslands in 2018. The crop field is located in Duolun County, Inner Mongolia (116.47°E, 42.18°, at 1269 m in altitude). The experimental area is approximately 50 m × 50 m and is surrounded by grasslands. Three types of crops, corn, oat (*Avena nuda*) and buckwheat, were planted and observed throughout the whole crop growth stage with a vehicle-mounted dual-polarized multi-frequency radiometer (RPG-6CH-DP). The radiometer could be lifted to a maximum height of 6.35 m above the ground to meet the requirement for far-field conditions. We designed two modes of observation: the daytime-scan mode and the nighttime-scan mode. The collection of observations from 10:00 to 20:59, the daytime-scan mode, was conducted at multiple azimuth angles and with a fixed incident angle of 55°. The collection of nighttime-scan mode observations, taken from 21:00 to 09:59, was conducted at multiple incident angles (from 30° to 65° with an interval of 2.5°) and with a fixed azimuth angle facing each crop type. Both modes of observation were triggered every half hour. Fig. 1a shows the footprint coverage of the nighttime-scan mode in the crop field. The crops sprouted at the end of June in 2017, and observations were taken continuously from July 19 to August 30, 2017. Unfortunately, the buckwheat was damaged by severe hail on August 11, 2017, and microwave radiometry data were lost from August 9 to August 17, 2017 due to memory failure. Considering the objectives of this study, only nighttime-scan data (with multiple incidence angles and multi-frequency) with better thermodynamic equilibrium in the corn field were used.

The grass field is located in Zhenglan Banner, Inner Mongolia (115.93°E, 42.04°, at 1362 m in altitude). The experimental area is an open, natural pasture with a coverage area of approximately 4 km^2. Observations of both microwave emissions and backscatter were conducted during the experiment. The measurements started on August 18, 2018 and ended on September 25, 2018. The ground incidence angle also ranged from 30° to 65° with an interval of 2.5°, and the azimuth angle included four directions to avoid the influence of surface heterogeneity, as shown in Fig. 1b. In this study, only microwave radiometry data were used, and these data were collected every half hour.

Details on the microwave radiation and ground parameter measurements are provided in Appendix A.

3. Methodologies

3.1. Degree of information

In information theory, the Shannon entropy, H, measures how much information is contained in a random variable X_i. For a set of N variables, $X_{1:N}$, the mutual information is the amount of information shared among the variables. For the multivariate case, the total correlation, $T(X_{1:N})$ (Watanabe, 1960), as one of many generalizations of mutual information, consists of all information that is shared among the variables and weights each piece according to how many variables it is shared among. The total correlation is expressed as the sum of the information contained in the individual variables (entropy of each variable, $H(X_i)$) minus the information contained in the whole set (joint entropy, $H(X_{1:N})$). The relevant equations are as follows:

$$H(X_i) = -\sum_{X_i} p(X_i) \cdot log_2 p(X_i) \tag{1}$$

$$H(X_{1:N}) = -\sum_{X_i} \cdots \sum_{X_N} p(X_{1:N}) \cdot log_2 p(X_{1:N}) \tag{2}$$

where $p(X_i)$ is the probability mass function of X_i and $p(X_{1:N})$ is the joint probability mass function of $X_{1:N}$.

$$T(X_{1:N}) = \sum_{i=1}^{N} H(X_i) - H(X_{1:N}) \tag{3}$$

Thus, the degree of nonshared information is proposed as the degree of information (*DoI*) by Konings et al., 2015.

$$DoI = N - \frac{T(X_{1:N})}{H(X_{1:N})} \tag{4}$$

For remote sensing, the *DoI* can be used to quantify the number of parameters that can be maximally estimated from a set of measurements. To be noted, a higher *DoI* means that more information can be utilized to estimate ground parameters, but it does not indicate that more parameters can be estimated definitely, as the actual number of estimated parameters should also depend on the signal-to-noise ratio and the performance of the retrieval algorithms, which determine how the signal of interest is extracted. However, the *DoI* is a good indicator to help design satellite configuration and retrieval algorithms for the use of multivariate information. In this study, we analyze how the *DoI* varies with multi-angular or multi-frequency measurements of brightness temperature, $Tb_{1:N}$, which is referred to as $X_{1:N}$.

3.2. Variance decomposition

The information contained in multi-angular and multi-frequency microwave observations consists of multiple contributors, including the land parameters of most interested: soil moisture and vegetation tau. To design an efficient retrieval algorithm, it is important to understand how and how much each land parameter explains the obtained microwave observations. In this study, we exploit variance decomposition (Gelman, 2005) across microwave observations into different variances of land parameters to help understand and utilize multi-angular and multi-frequency information. Here, the general linear regression model for variance decomposition is formulated as follows:

$$Y = a \cdot VWC + b \cdot SM + c \cdot VWC \cdot SM + d + \varepsilon \tag{5}$$

where Y is the response variable (microwave observation) to be analyzed; VWC is the vegetation water content; SM is the soil moisture; $a \cdot VWC$, $b \cdot SM$, and $c \cdot VWC \cdot SM$ are the vegetation contribution term, the soil contribution term and the soil-vegetation interaction term, respectively; d is a constant; and ε is the residual. For the regression analysis, the determination coefficient R^2 is usually defined as the fraction of variance explained, as follows:

$$R^2 = \frac{SS_{explained}}{SS_{total}} = 1 - \frac{SS_{\varepsilon}}{SS_{total}} = 1 - \eta_{\varepsilon}^2 \tag{6}$$

where SS_{total} is the total sum of squares (proportional to the variance of the data) of the response variable; $SS_{explained}$ is the explained sum of squares; SS_{ε} is the residual sum of squares, which is also called the unexplained sum of squares; and η_{ε}^2 is the proportion of variance that is

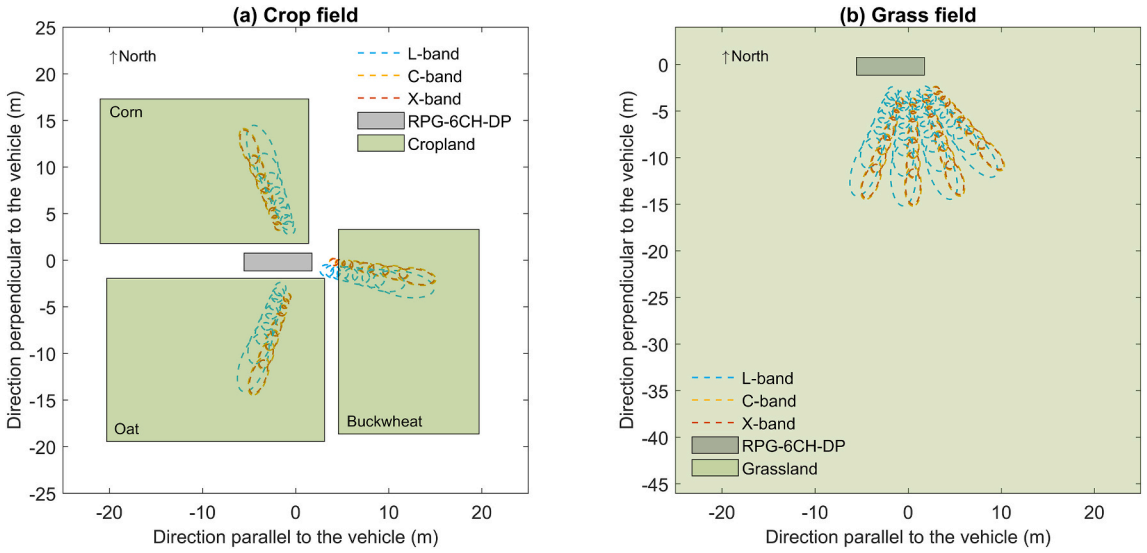

Fig. 1. Experimental setup of the ground-based measurements obtained by microwave radiometry. Colored ellipses show the ground footprints varying with the azimuth angle and incidence angle from 30° to 65°. Green patches show the experimental fields, and the grey patch represents the vehicle carrying the RPG-6CH-DP radiometer. (For interpretation of the references to colour in this figure legend, the reader is referred to the web version of this article.)

unexplained.

Similarly, the proportion of variance explained by each contribution term can be represented as follows:

$$\eta^2_{VWC} = \frac{SS_{VWC}}{SS_{total}} \tag{7}$$

$$\eta^2_{SM} = \frac{SS_{SM}}{SS_{total}} \tag{8}$$

$$\eta^2_{VWC\cdot SM} = \frac{SS_{VWC\cdot SM}}{SS_{total}} \tag{9}$$

Notably, $\eta^2_{VWC} + \eta^2_{SM} + \eta^2_{VWC\cdot SM} + \eta^2_{\varepsilon}$ may not be equal to 1, as the soil moisture and vegetation water content are not completely independent.

For passive microwave remote sensing, the normalized polarization difference index (NPDI), normalized frequency difference index (NFDI), and normalized angular difference index (NADI) are used as the response variables, Y, to analyze their variance decomposition and understand how information from the polarization (P), incidence angle (θ), and frequency (f) responds to changes in the soil moisture and vegetation water content. One strength of these indices is that they minimize the impact of uncertainties in surface physical temperatures.

3.2.1. NPDI

The NPDI is proposed to quantify the polarization difference at a given single angle and frequency. The NPDI is also referred to as the microwave polarization difference index (MPDI, Becker and Choudhury, 1988) or the polarization index (PI, Paloscia and Pampaloni, 1992).

$$NPDI = \frac{Tb_V - Tb_H}{Tb_V + Tb_H} \tag{10}$$

The NPDI, as derivation in Meesters et al., 2005, is affected not only by vegetation properties (vegetation tau and single scattering albedo) but also by soil reflectivity (soil moisture and surface roughness). The NPDI has been widely used in the retrieval of soil moisture and vegetation tau (Owe et al., 2001; De Jeu and Owe, 2003; Owe et al., 2008; De Jeu et al., 2008; Parinussa et al., 2012).

3.2.2. NFDI

The NFDI is defined to quantify the brightness temperature difference between two frequencies at a specific polarization.

$$NFDI = \frac{Tb_{P,f_1} - Tb_{P,f_2}}{Tb_{P,f_1} + Tb_{P,f_2}} \tag{11}$$

The NFDI has been referred to as an index of soil moisture (ISW) and was described for AMSR-E soil moisture retrievals (Koike et al., 2004; Fujii et al., 2009). It has also been referred to as the emissivity difference vegetation index for applications in dense forest conditions (Min and Lin, 2006).

3.2.3. NADI

Similarly, we further define the NADI to quantify the brightness temperature difference between two incidence angles at a specific polarization.

$$NADI = \frac{Tb_{P,\theta_1} - Tb_{P,\theta_2}}{Tb_{P,\theta_1} + Tb_{P,\theta_2}} \tag{12}$$

3.3. Retrieval approach

3.3.1. Algorithm description

In previous studies, based on the two-component version of the omega-tau model (Appendix B), Shi et al., 2008 developed microwave vegetation indices (MVIs) to minimize the soil contribution by assuming that the rough soil emissivity at two adjacent AMSR-E frequencies are linearly correlated. Zhao et al., 2011 analytically derived the vegetation transmissivity (vegetation water content) from the MVIs when the single scattering albedo was assumed to be zero and the vegetation effects were polarization-independent. Furthermore, we have extended this analytical derivation to the multi-angular configuration of SMOS (Shi et al., 2019). Although an analytical solution of vegetation transmissivity (or the vegetation transmission term) could be derived in our original studies, the assumptions are too limited to make these derivations applicable at a global scale, as the vegetation signals should be polarization-, incidence angle- and frequency-dependent.

In contrast to previous studies (Zhao et al., 2011; Li et al., 2015; Cui et al., 2015), we derived a new relationship of the total observed brightness temperature at any two channels without any assumptions. Based on the two-component omega-tau model (see Appendix B), we performed the following calculation:

$$Tb^{total}_{ch} = V^e_{ch} + V^t_{ch} \cdot e^s_{ch} \tag{13}$$

where *ch* denotes different channels, hereafter used to indicate the polarization (*P*), incidence angle (θ) and frequency (*f*); Tb_{ch}^{total} is the total brightness temperature observed at channel *ch*; e_{ch}^{s} is the emissivity of the rough soil surface as a function of the soil dielectric constant ε_{ch}^{s} and the surface roughness *Rou*; V_{ch}^{e} is the vegetation emission term; and V_{ch}^{t} is the vegetation transmission term. These vegetation contribution terms are mainly related to the vegetation coverage F_v, effective single scattering albedo ω_{ch} and effective vegetation optical depth (tau) τ_{ch}, as described in detail in Appendix B.

Then, the rough soil emissivity is derived:

$$e_{ch(1)}^{s} = \frac{Tb_{ch(1)}^{total} - V_{ch(1)}^{e}}{V_{ch(1)}^{t}} \tag{14}$$

$$e_{ch(2)}^{s} = \frac{Tb_{ch(2)}^{total} - V_{ch(2)}^{e}}{V_{ch(2)}^{t}} \tag{15}$$

Dividing Eq. (14) by Eq. (15), we obtain:

$$F_{cond} : Tb_{ch(2)}^{total} = V_{ch(2)}^{e} - S_r V_r \cdot V_{ch(1)}^{e} + S_r V_r \cdot Tb_{ch(1)}^{total} \tag{16}$$

and

$$S_r = \frac{e_{ch(2)}^{s}}{e_{ch(1)}^{s}} \tag{17}$$

$$V_r = \frac{V_{ch(2)}^{t}}{V_{ch(1)}^{t}} \tag{18}$$

where *ch* denotes different channels in terms of the polarization, incidence angle, and frequency; S_r is the ratio of soil emissivity as a function of soil moisture (*SM*) and surface roughness (*Rou*); and V_r is the ratio of the vegetation transmission term. Eq. (16) indicates that, for a given brightness temperature and corresponding soil and vegetation parameters, the brightness temperature at another channel can be predicted. Therefore, Eq. (16) can serve as a key conditional restriction when multi-channel information is available.

As soil moisture and surface roughness can be measured in the field, they are treated to be independent from the microwave observations. The effective single scattering albedo and vegetation tau can be estimated from passive microwave observations or simulations. Therefore, for a given brightness temperature observation at one channel, the unknown parameters are $\{SM, Rou, \omega_{ch(1)}, \tau_{ch(1)}\}$. In the framework of a zero-order approximation, the vegetation signals represented by the effective single scattering albedo and vegetation tau are polarization-, incidence angle- and frequency-dependent. When more information (brightness temperature) from other channels is available, the unknown parameters increase to include $\{SM, Rou, \omega_{ch(1)}, \tau_{ch(1)}, \omega_{ch(2)}, \tau_{ch(2)}, \ldots, \omega_{ch(N)}, \tau_{ch(N)}\}$. Without any assumptions, there are always more unknowns $(2 \cdot N + 2)$ than observations (*N*), which makes the retrieval an ill-posed problem. To perform the retrieval, the number of unknowns must be reduced. Therefore, the vegetation tau at any two channels (*ch*: polarization, incidence angle and frequency) is expressed as the following function (Ulaby et al., 1983; Jackson and Schmugge, 1991; Wigneron et al., 2007; Zhao et al., 2011):

$$F_{asm} : \frac{\tau_{ch(1)}}{\tau_{ch(2)}} = \left(\frac{f_1}{f_2}\right)^{C_f} \cdot \frac{sin^2\theta_1 \cdot C_{P_1} + cos^2\theta_1}{sin^2\theta_2 \cdot C_{P_2} + cos^2\theta_2} \tag{19}$$

where $C_f > 0$, $C_P > 0$ are parameters characterizing the dependence of τ_{ch} on frequency and polarization, respectively, and should be dependent on the vegetation type (Baur et al., 2019). It has been reported that $C_f = 0.5$ in Pampaloni and Paloscia, 1986, and that $C_f = 1.08$ for wheat and $C_f = 1.38$ for soybeans (Jackson and Schmugge, 1991). The "isotropic" case, $C_P = 1$, corresponds to the assumption used in this study that the vegetation tau is independent of both the polarization and incidence angle ($\tau_V = \tau_H = \tau^0$ *at nadir*), which is a commonly used assumption in previous studies (Wigneron et al., 2004; Kerr et al., 2012; Fernandez-Moran et al., 2017a).

With site-specific roughness parameter (*Rou*) and single scattering albedo ($\omega_{ch(1:N)}$) values, the unknown parameters are $\{SM, \tau_{ch(1)}\}$. The retrieval approach can be carried out in traversal form as follows:

i. Generation of candidate parameters: Assuming a set of soil moisture values (e.g., from 0.001 cm^3/cm^3 to the porosity of the soil), a set of vegetation tau values $\tau_{ch(1)}$ could be calculated from $Tb_{ch(1)}^{total}$ at the core channel with an assumed soil moisture value and given $\{Rou, \omega_{ch(1)}\}$ parameters through a reverted omega-tau model ($F_{\omega-\tau}^{-1}$, Appendix C). With the assumption on vegetation tau at different channels, $\tau_{ch(2:N)}$ values are obtained for other channels with F_{asm} of Eq. (19).
ii. Conditional restrictions calculation: With the input parameters $\{SM, Rou, \omega_{ch(2:N)}, \tau_{ch(2:N)}\}$, the brightness temperatures $Tb_{ch(2:N)}^{estimated}$ at other collaborative channels can be calculated with F_{cond} of Eq. (16).
iii. Retrieval by minimizing the cost function: Pearson's chi-squared error is used to describe the difference between the observed and estimated brightness temperatures, and the soil moisture and corresponding vegetation tau $\{SM, \tau_{ch(1)}\}$ values are retrieved when the cost function approaches the minimum, calculated as follows:

$$min\Phi : \sum_{i=2}^{N} W_i \cdot \frac{\left(Tb_{ch(i)}^{estimated} - Tb_{ch(i)}^{total}\right)^2}{Tb_{ch(i)}^{total}} \tag{20}$$

where $Tb_{ch(i)}^{total}$ is the observed brightness temperature at the $i-th$ channel *ch* (polarization, incidence angle and frequency) and $Tb_{ch(i)}^{estimated}$ is the estimated brightness temperature at the $i-th$ channel *ch*. Weights, W_i, could be applied to obtain the weighted sums of the contributions from different collaborative channels.

The above algorithm could also be implemented in iterative form, which may enable the retrieval of more unknowns $\{SM, Rou, \omega_{ch(1)}, \tau_{ch(1)}\}$ with enough observations from different channels. In this algorithm, the brightness temperature at the core channel is used to generate a sequence of candidate parameters, and the brightness temperatures at other collaborative channels are used to find the approximated solutions by minimizing a cost function. Therefore, it is hereafter referred to as a multi-channel collaborative algorithm (MCCA), and the flowchart of this MCCA is given in Fig. 2.

3.3.2. Algorithm implementation

For the implementation of the MCCA in this study, the effective single scattering albedo is specified to be 0, 0.06 and 0.08 for the L-, C- and X-bands, respectively, in the corn field, and it is assumed to be 0 for all bands in the grass field. These specified values are reasonable compared to those used in previous studies, in which it was found that the (effective) single scattering albedo of corn ranges from 0 to 0.17 at L-band, from 0.05 to 0.08 at C-band, and is approximately 0.08 at X-band; it was also found to range from 0 to 0.05 at L-band for grass (Mo et al., 1982; Ulaby et al., 1983; Pampaloni and Paloscia, 1986; Van De Griend and Wigneron, 2004; Wigneron et al., 2004; Zhao et al., 2020b). The polarization dependence parameter is considered to be $C_P = 1$, indicating that the vegetation tau is polarization- and incidence angle-independent, and the frequency dependence parameter is considered to be $C_f = 0.6$ for the corn field and $C_f = 1$ for the grass field. The effects of the uncertainty of these vegetation type-dependent parameters on the retrievals are not considered in this study.

The soil and vegetation temperatures are assumed to be equal to the effective soil temperature T_s^{eff}. The estimation of the effective soil temperature refers to a parametric formulation, as follows (Choudhury et al., 1982; Wigneron et al., 2001):

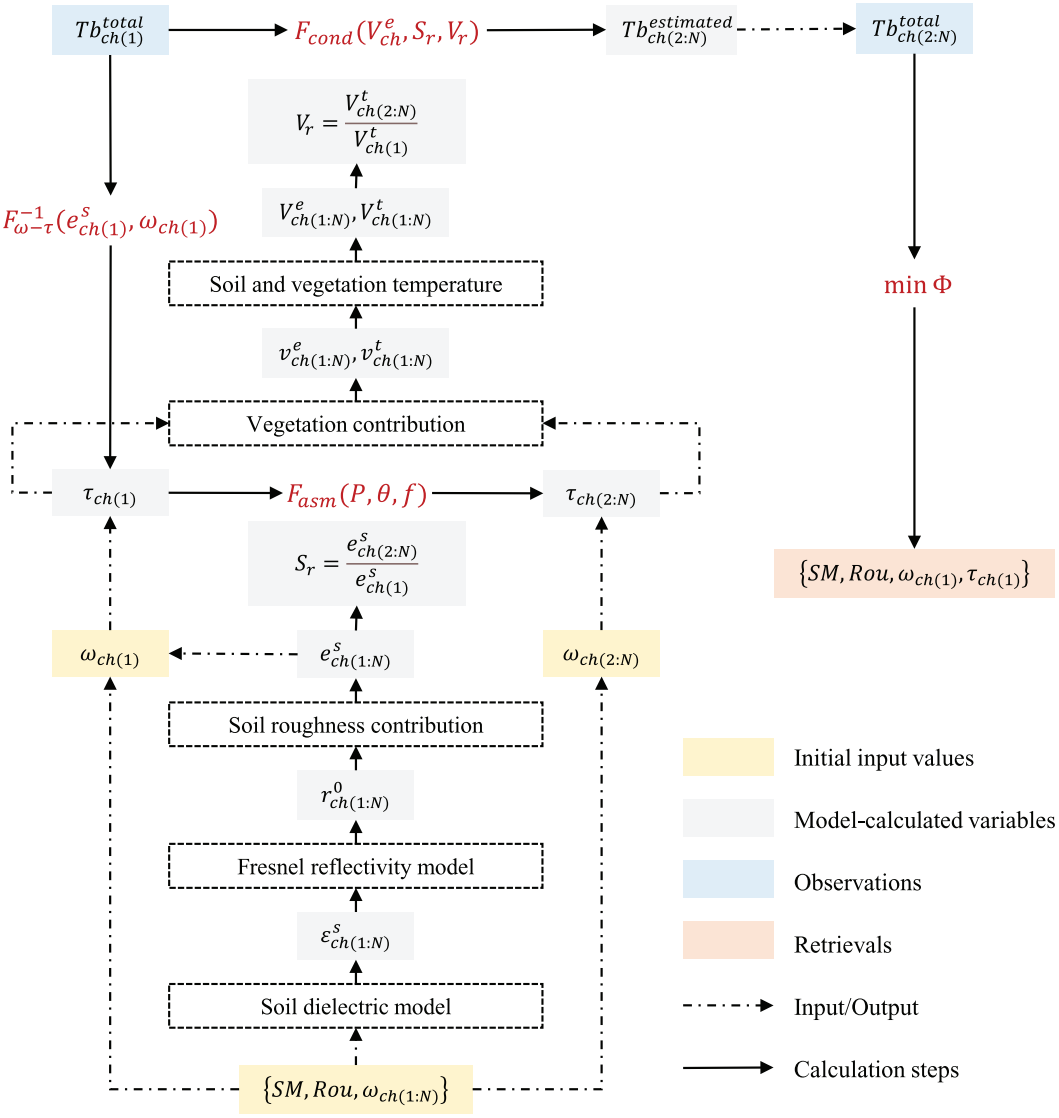

Fig. 2. Flowchart illustrating the theoretical basis of the multi-channel collaborative algorithm (MCCA).

$$T_s^{eff} = T_s^{depth} + \left(T_s^{surf} - T_s^{depth}\right) \cdot \left(\frac{SM}{w_0}\right)^{b_{w0}} \tag{21}$$

where T_s^{surf} is the soil temperature at the surface (0–5 cm) and T_s^{depth} is the soil temperature at depth (50–100 cm). As the soil is very sandy in our experimental area, the parameters are set to $w_0 = 0.7315$ and $b_{w0} = 0.18941$ in this study; these values are derived from previous studies (Wigneron et al., 2008). In this study, soil temperatures measured at depths of 2.5 cm in the corn field (3 cm in the grass field) and 50 cm were used to calculate the effective soil temperature.

For the soil surface roughness effects, there have been various models that include theoretical and semi−/empirical models. Among these models, the most commonly used semi-empirical model is the QHN model (Wang and Choudhury, 1981), expressed as follows:

$$r_p^s = \left[(1-Q)\cdot r_p^0 + Q\cdot r_q^0\right]\cdot exp\left(-h\cdot cos^N\theta\right) \tag{22}$$

where r_p^s and r_p^0 are the reflectivity of the rough soil surface and smooth surface, respectively; Q is the polarization decoupling factor; h is the roughness parameter; and N is a parameter used to account for the angular dependence. It is normally considered that $Q = 0$ at L-band (Wigneron et al., 2001; Lawrence et al., 2013; Zhao et al., 2015a). As the frequencies increase (from C- to Ka-band), the only Q parameter can be used to describe the roughness effects at larger incidence angles (Shi et al., 2005). As in this study, we are dealing with multi-angular and multi-frequency configurations, the Q/H/N parameters were optimized with ground-based measurements at the beginning of the crop experiment (bare soil) by minimizing the difference between the modelled and measured brightness temperatures. Calibrated constant values ($Q = 0.0327$, $h = 0.0967$ at L-band, $Q = 0.2783$, $h = 0.1042$ at C-band, $Q = 0.3143$, $h = 0.2018$ at X-band; and $N = 2$) are used since no special treatment of surface roughness was made during the whole experiment.

The Mironov model (Mironov et al., 2004) is utilized for the calculation of soil dielectric constants under different soil moisture content.

4. Results and discussion

4.1. Information contained in multi-angular and multi-frequency observations

Remotely sensing ground parameters is often an ill-posed problem, as the same observation may be explained by different sets of environmental factors. To improve the robustness of retrievals, it is necessary to increase the information contained in the observations. In this study, we

analyze the *DoI* contained within multi-angular and multi-frequency observations. It is argued that a higher *DoI* may indicate more possibilities to perform a robust retrieval (Konings et al., 2015), which truly depends on whether the parameters to be retrieved change with the observations or not.

Fig. 3a, b and c present the *DoI* variations with dual-angle combinations for the L-, C- and X-bands, repetitively. Generally, the *DoI* increases as the incidence angle increases due to the increasing polarization difference. A larger *DoI* is presented between two more distant angles, especially at X-band. It is expected that the vegetation properties in terms of the path/depth penetrated by two more distant angles are more different that those penetrated by two angles that are closer to each other. Conversely, observations from two closer angles contain less independent information (smaller *DoI*), which means that the two observations are more highly correlated. It is noted that with the dual-angle combination, the L-band contains more information (larger *DoI*) than do the C- or X-bands. This may indicate that for multi-angular configuration (e.g., SMOS), the L-band has a larger sensitivity to the overall vegetation plant and soil moisture, and it is an optimal band for soil moisture retrievals compared to the C- and X-bands.

Fig. 4 presents the *DoI* variations that occur with different frequency combinations for different incidence angles. The *DoI* reaches its maximum around Brewster's angle (from 55° to 62.5°), at which the polarization difference is greatest. This indicates that it might be optimal to operate around the Brewster angle for satellite missions (e.g., SMAP or CIMR) with fixed viewing angles; however, trade-offs must be made, as it can be easier to achieve saturation for dense vegetation. Except for at Brewster's angle, the V- and H-pol measurements have reduced distinctions and hence contain lower amounts of independent information (smaller *DoI*) when the incidence angle is decreased. For the configuration with a single frequency and a single incidence angle, there is no significant advantage with the L-band in terms of *DoI*, while the frequency combination with the L-band (L- and C-band, L- and X-band) shows a larger *DoI* than that of the C- and X-band combination.

When the number of variables (observations at different incidence angles or frequencies) increases, the *DoI* should increase accordingly. In Fig. 5, the *DoI* values that occur under various combinations and their relationships with the numbers of variables are presented. A numerical table complementing Fig. 5 of all *DoI* obtained for given numbers of channels is summarized in Table 2. For example, as seen in Fig. 5a, there are a total of C_{15}^{5} possible combinations of 5 incidence angles from a set of 15 incidence angles (from 30° to 65° with an interval of 2.5°). The *DoI* was calculated for all these possible combinations and plotted as colored dots. It can be found that there is a clear linear relationship between the *DoI* and the number of variables, while no saturation is found based on our experimental data. The *DoI* can be expressed as follows:

$$DoI = \alpha \cdot N + \beta \tag{23}$$

where N is the total number of variables and α, β are coefficients of the linear function. The linearity might imply that there should be many more environmental variables/parameters than only the soil moisture and vegetation water content, such as the leaf radius, leaf thickness, stalk length, stalk density, etc. as well as distributions of those dielectric elements, affecting the total brightness temperature emitted from the ground. In addition, the ground objects (dielectric elements) and their features "seen" by the radiometer under different channels are actually different from each other, as affected by differences in the penetration ability, field of view and viewing angle. The differentiation of ground objects and the complexity of the objects themselves lead to a linear increase in the *DoI*. It is worth mentioning that it is important to use both H- and V-pol, which together have a clearly larger *DoI* than do single polarizations. Additionally, the *DoI* can be largely increased when more angles are considered. Further, it is found that the slope of the linear relationship for increasing numbers of frequencies (0.7306 for single polarization and 1.4111 for dual polarization) is slightly higher than that for increasing numbers of incidence angles (0.666 for single polarization and 1.3322 for dual polarization). This means that for the same number of variables/observations from a given satellite, more independent information might be provided with the multi-frequency configuration (e.g., CIMR) rather than with the multi-angular configuration (e.g., SMOS). However, the SMOS mission can easily obtain observations at dozens of incidence angles and should provide more independent information than the CIMR mission, which only has a limited number of frequencies, as the *DoI* increases linearly with an increasing number of channels. In terms of soil moisture retrievals, there is no guarantee that more robust results can be retrieved for higher *DoI* values, as the robustness of retrieval depends on the characteristics of the unknowns, the RTE and the retrieval algorithm used, which is discussed in Sections 4.3–4.5.

4.2. Decomposition into soil moisture and vegetation water content

As mentioned above, information contained within microwave observations includes various environmental factors, and only the information that varies with (is explained by) soil moisture or vegetation properties can be utilized for accurate retrievals. Thus, researchers have developed many methodologies and indices (e.g., NPDI, MVIs, etc.) with which to maximize the information of targeted parameters and minimize the effects from other environmental factors. In this study, we explore the differences in brightness temperatures between polarization, incidence angle and frequency through variance decomposition into soil moisture and vegetation water content.

Fig. 6 shows the proportion of the NPDI variance explained by the vegetation water content, soil moisture, soil-vegetation interaction and residuals at L-, C- and X-bands, respectively. For the L-band NPDI, the

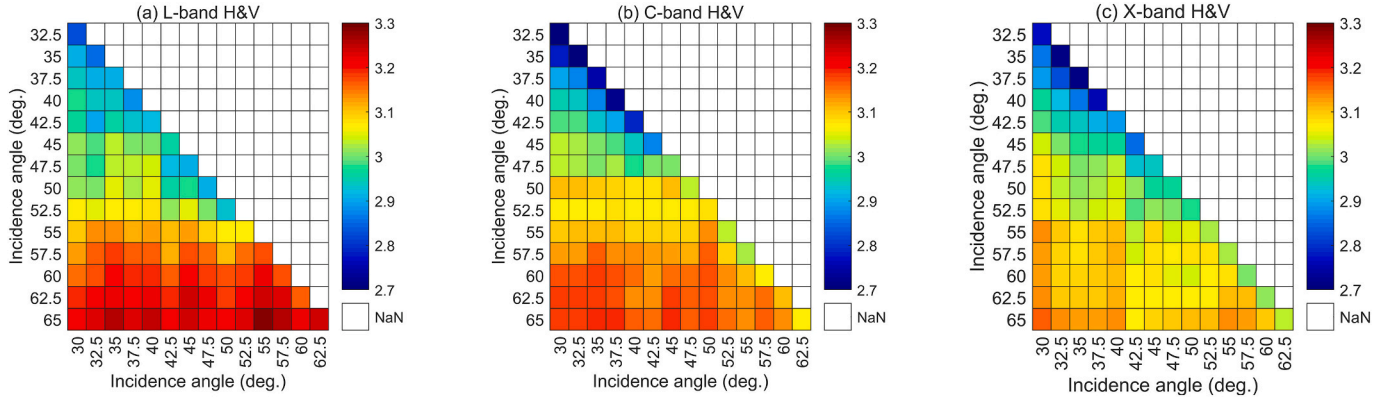

Fig. 3. Degree of information of dual-angle combinations with dual-polarization observations at L- (a), C- (b) and X-bands (c) in the corn field. The colour bars represent the values of the degree of information.

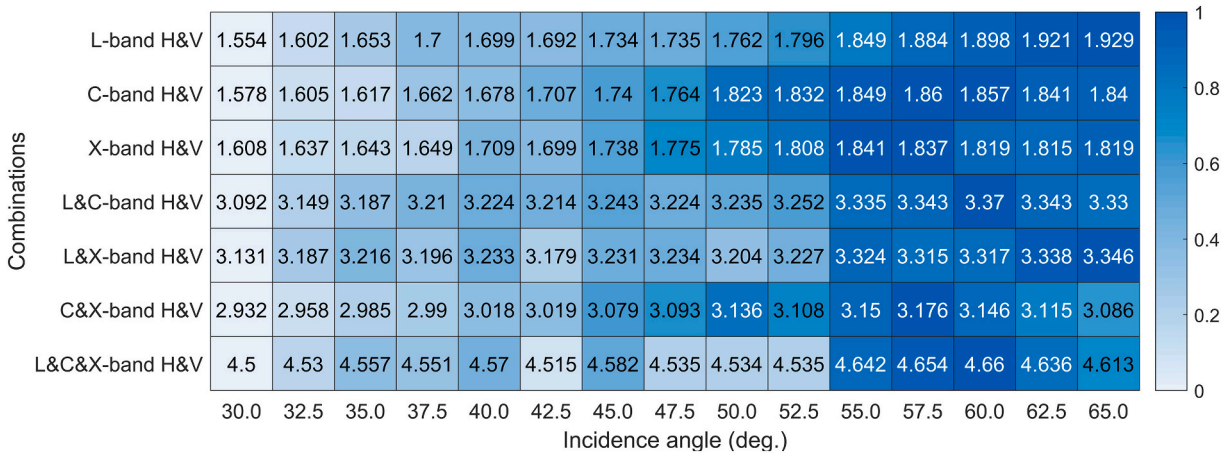

Fig. 4. Degree of information of multi-frequency combinations with dual-polarization observations at different incidence angles in the corn field. The colour bar represents the value of the degree of information, and the colour is scaled row-wise to values from 0 to 1.

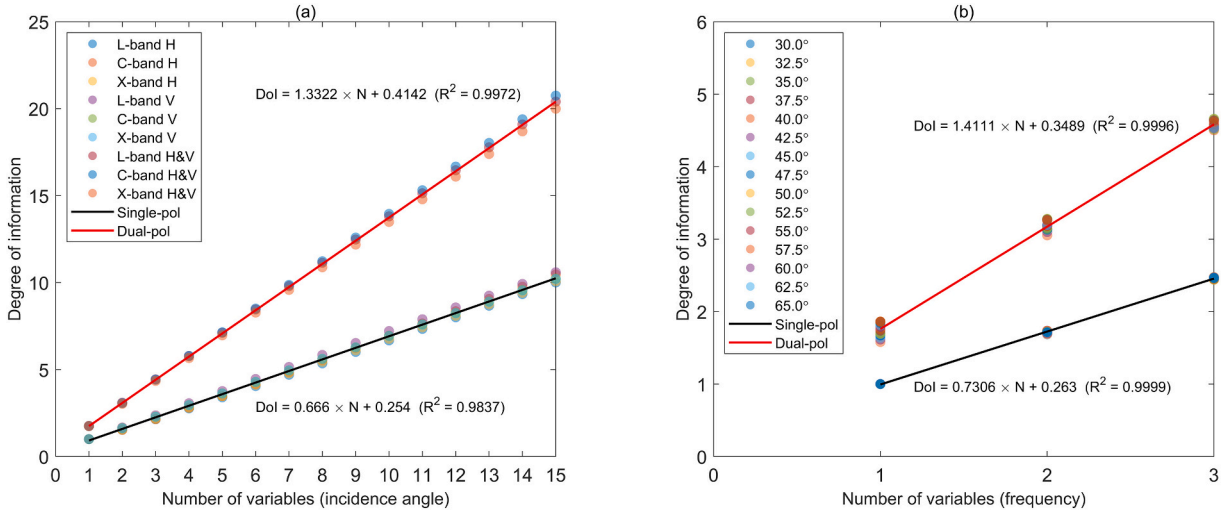

Fig. 5. Degree of information in the corn field as a function of the number of variables, which are observations of brightness temperatures at different incidence angles (a) or frequencies (b). Colored dots present the degree of information under different combinations (incidence angles or frequencies). The red line is the fitted linear relationship between the degree of information and the number of variables for the dual-polarization observations, and the black line is that for single-polarization observations. (For interpretation of the references to colour in this figure legend, the reader is referred to the web version of this article.)

Table 2
DoI in the corn field with increasing numbers of channels in terms of polarization, incidence angle and frequency (SD is the standard deviation of ***DoI*** for all possible combinations).

Number of Channels	Single polarization				Dual polarization			
	Incidence angle		Frequency		Incidence angle		Frequency	
	Mean	SD	Mean	SD	Mean	SD	Mean	SD
1	1.000	0.000	1.000	0.000	1.752	0.008	1.752	0.098
2	1.590	0.057	1.711	0.015	3.066	0.031	3.187	0.071
3	2.234	0.092	2.461	0.011	4.401	0.047	4.574	0.054
4	2.894	0.115			5.738	0.067		
5	3.560	0.132			7.075	0.092		
6	4.229	0.145			8.411	0.120		
7	4.899	0.156			9.746	0.148		
8	5.569	0.165			11.081	0.177		
9	6.240	0.174			12.414	0.206		
10	6.911	0.182			13.746	0.235		
11	7.581	0.190			15.076	0.263		
12	8.252	0.199			16.405	0.291		
13	8.922	0.207			17.732	0.319		
14	9.592	0.216			19.057	0.347		
15	10.262	0.226			20.381	0.376		

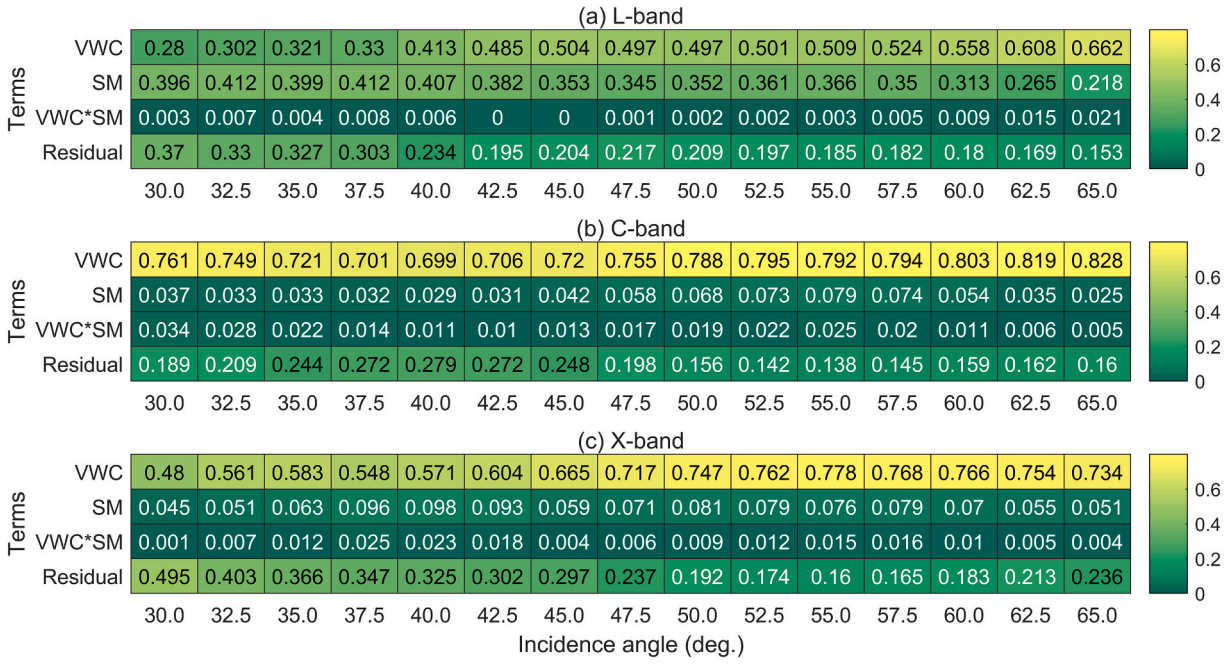

Fig. 6. Proportions of the NPDI variance explained by each contributing term (η^2_{VWC}, η^2_{SM}, $\eta^2_{VWC\cdot SM}$ and η^2_{ϵ}) at L- (a), C- (b) and X-bands (c) under different incidence angles, as observed in the corn field.

proportion of variance explained by the vegetation water content is slightly higher than that explained by the soil moisture. With an increasing incidence angle, the proportion of the variance explained by vegetation increases, and the soil-moisture explained variance generally decreases. It is expected that the vegetation tau becomes larger at larger incidence angles. The contribution of the soil-vegetation term is generally small, and more variance in the NPDI could be explained by the linear regression model at larger incidence angles. For the C- and X-band NPDI, similar patterns of variance distribution are presented, as the vegetation water content explains most of the variance in both bands. The soil moisture only explains a small proportion of the variance, with a value below 0.1, which is attributed to the reduced penetration abilities of vegetation at C- and X-bands. Generally, the polarization difference is mainly explained by the vegetation water content in the corn field and should perform better at L-band (e.g., SMAP mission) for a soil moisture algorithm that utilizes polarization information.

Fig. 7 shows the proportions of the NFDI variance explained by the vegetation water content, soil moisture, soil-vegetation interaction and residuals at different combinations of frequencies. The L- & C-bands and C- & X-bands, which represent combinations of two adjacent frequencies, present similar variance distribution patterns in which the soil moisture generally explains a larger part of the total variance in the NFDI than the vegetation water content does, with the exception of the incidence angle at 65°. This pattern is more significant between the incidence angles 40° and 55°. This means that the brightness temperature difference between two adjacent frequencies is mainly caused by the soil moisture. However, the vegetation water content explains a larger part of the NFDI variance than the soil moisture does for the L- & X-band combination. It is reasonable that the vegetation tau is differentiated between the L- and X-bands. These results may indicate that the observed brightness temperature differences between adjacent frequencies (e.g., CIMR mission) could be used for soil moisture retrievals, and this difference is used as a soil moisture index in the algorithm developed by JAXA for the AMSR-E and AMSR2 sensors.

Fig. 8 shows the proportions of the NADI variance explained by the vegetation water content, soil moisture, soil-vegetation interaction and residuals at different incidence-angle combinations. It is very interesting to observe that the soil moisture information is minimized with low proportions of variance (from 0 to 0.186) explained by soil moisture for all L-, C- and X-bands. This is true because, assuming there is a linear decreasing relationship between the H-pol brightness temperature and incidence angle, changes in vegetation mainly affect the slope (Talebiesfandarani et al., 2019), which changes the NADI, while soil moisture changes mainly affect the intercept of the linear relationship. The proportion of variance explained by the vegetation water content increases for the L-band but decreases for the C- and X-bands as the incidence angle increases. Unfortunately, the unexplained variance also has a large proportion, especially for the C-band H-pol observations, as observed in the corn field. These results may indicate that brightness temperature differences between incidence angles (e.g., SMOS mission) could be utilized for retrieving vegetation properties.

The analysis above has shown that the information provided by brightness temperature differences among different polarizations, frequencies and incidence angles has distinguished characteristics in terms of responding to vegetation and soil moisture changes. Currently, the NPDI has been widely used in retrievals of soil moisture and vegetation tau, while few studies have reported using the NFDI and NADI, both of which need further investments for their adoption in algorithms.

4.3. Retrievals in the corn field

The soil moisture and vegetation tau values were first retrieved based on the multi-angular approach at L-band with single H-pol or dual-pol observations. Performance metrics, including the correlation coefficient (R), bias, and unbiased root mean square difference (ubRMSD) with their respective 95% confidence intervals (Gruber et al., 2020), are listed in Table 3.

For the single H-pol retrievals, which follow a pure multi-angular approach, the results with brightness temperatures from 40° and 55°, 50° and 65°, and 40° to 65° are shown in Fig. 9, Fig. 10, and Fig. 11, respectively. It can be seen that soil moisture and vegetation tau can be retrieved simultaneously with brightness temperatures at two different incidence angles, even though the results might not be sufficiently robust, as the *DoI* is less than 2. However, for the case with only dual-channel information, it is also possible to perform a reliable retrieval, as the MCCA first generates a series of paired candidate parameters (soil

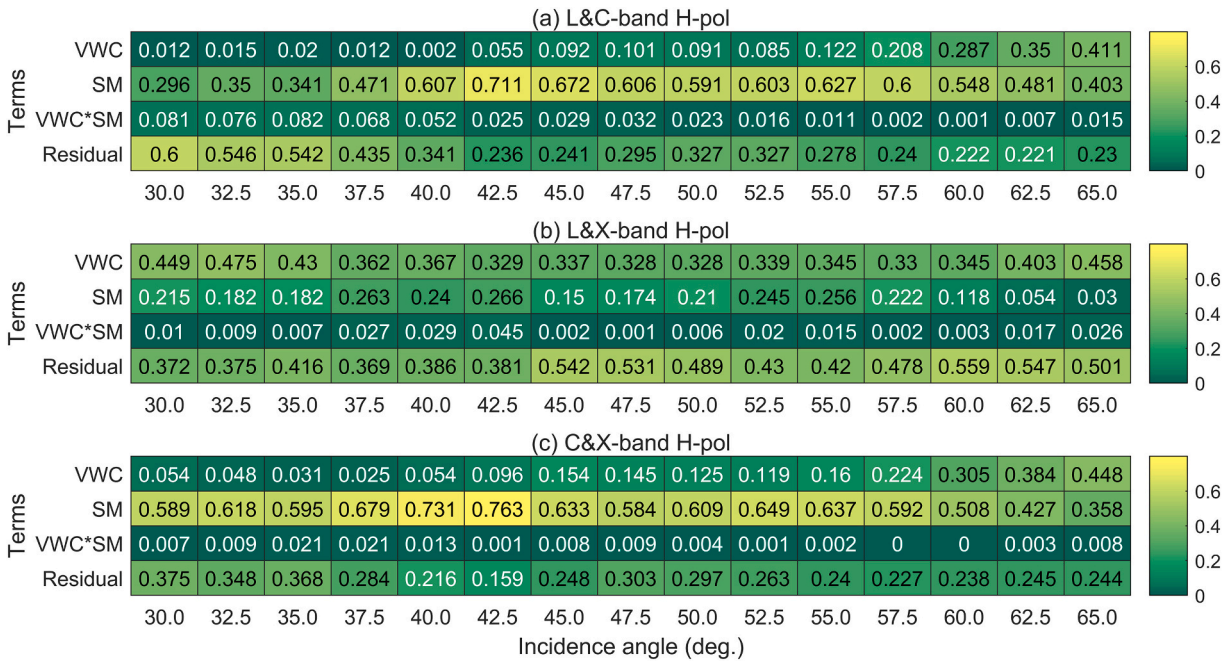

Fig. 7. Proportions of the NFDI variance explained by each contributing term ($\eta^2_{\bar{V}WC}$, η^2_{SM}, $\eta^2_{\bar{V}WC \cdot SM}$ and η^2_{ε}) at L- & C-bands (a), L- & X-bands (b) and C- & X-bands (c) under different incidence angles, as observed in the corn field.

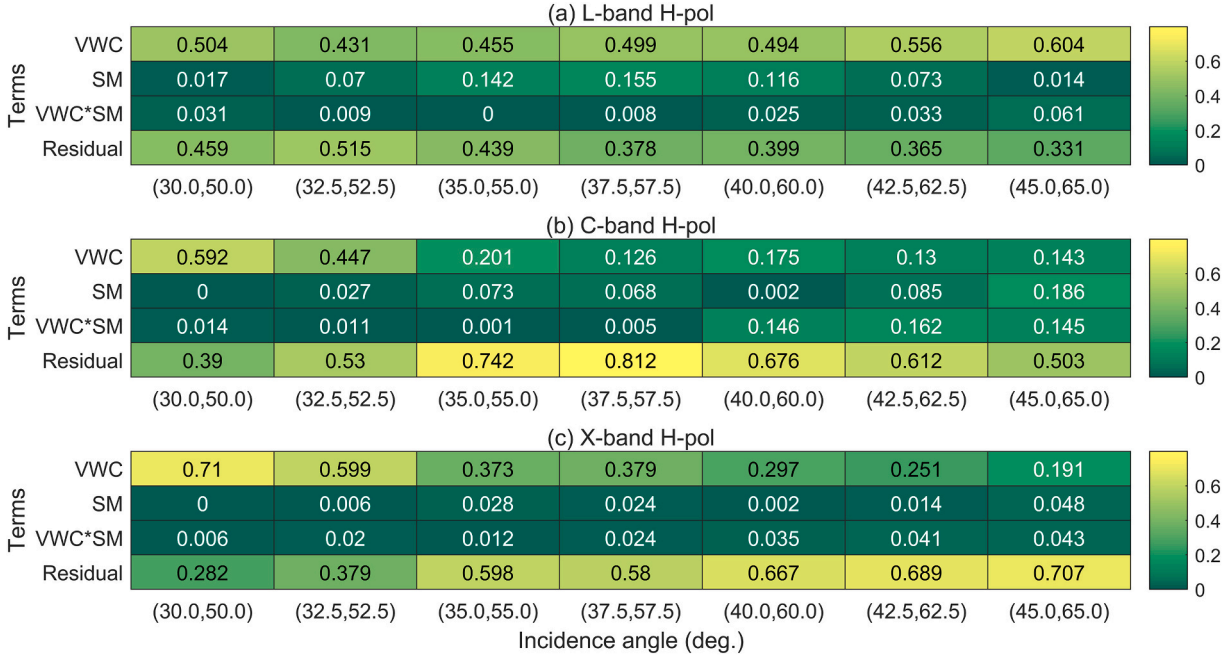

Fig. 8. Proportions of the NADI variance explained by each contributing term ($\eta^2_{\bar{V}WC}$, η^2_{SM}, $\eta^2_{\bar{V}WC \cdot SM}$ and η^2_{ε}) at L- (a), C- (b) and X-bands (c) under different incidence-angle combinations, as observed in the corn field.

moisture and tau) by using the brightness temperature from the core channel and then rules out the "right" parameters to be retrieved using the cost function of the collaborative channel. Soil moisture retrievals from dual-channel observations (40° and 55°, L- and C-band at 45°, H-pol only) show a minimum ubRMSD of 0.028 cm^3/cm^3 when compared to in situ measurements at 2.5 cm. As the incidence angle increases, the retrieved soil moisture becomes wetter, with the bias moving from a negative value towards a positive value for both H-pol and dual-pol, while the ubRMSD at H-pol increases to 0.037 cm^3/cm^3 with observations at 50° and 65°. The wetter values resulting from larger incidence angles might partly result from the fact that the brightness temperatures observed by the radiometer at larger incidence angles receive signals radiated from the sky, which lowers the observed brightness temperatures and leads to wetter soil moisture results. This might also be partly due to the increased scattering effects that occur at larger incidence angles, and underestimating effective single scattering albedo (constant value of 0) leads to an overestimation of soil moisture. As only one location was selected to measure the soil moisture and temperature for each crop field, the spatial heterogeneity of the soil and vegetation properties is also possibly one of the reasons for this uncertainty.

Table 3
Retrieval performances in the corn field. [X_l X_u] rows are the 95% confidence intervals of the X (being R, Bias, ubRMSD) estimates.

Configuration	Number	R		Bias		ubRMSD		R
		R_l	R_u	Bias_l	Bias_u	ubRMSD_l	ubRMSD_u	
		Soil moisture						Tau
L-band H-pol	504	0.574		−0.024		0.028		0.362
40° and 55°		0.512	0.630	−0.027	−0.022	0.026	0.030	
L-band Dual-pol	538	0.498		−0.016		0.034		0.365
40° and 55°		0.432	0.559	−0.019	−0.013	0.032	0.036	
L-band H-pol	554	0.557		−0.008		0.032		0.514
45° and 60°		0.497	0.612	−0.011	−0.006	0.030	0.034	
L-band Dual-pol	572	0.584		−0.001		0.033		0.522
45° and 60°		0.527	0.635	−0.004	0.001	0.031	0.035	
L-band H-pol	572	0.717		0.029		0.037		0.861
50° and 65°		0.675	0.755	0.025	0.032	0.035	0.039	
L-band Dual-pol	572	0.732		0.039		0.034		0.852
50° and 65°		0.692	0.768	0.036	0.042	0.033	0.037	
L-band H-pol	545	0.657		−0.012		0.030		0.687
40° to 65°		0.606	0.702	−0.015	−0.009	0.028	0.032	
L-band Dual-pol	551	0.659		−0.009		0.031		0.676
40° to 65°		0.609	0.704	−0.012	−0.007	0.029	0.033	
L- and C-band	503	0.675		−0.024		0.028		0.446
H-pol 45°		0.624	0.720	−0.027	−0.022	0.026	0.030	
L- and C-band	572	−0.278		0.045		0.055		0.591
Dual-pol 45°		−0.352	−0.200	0.041	0.050	0.052	0.058	
L- and X-band	482	0.585		−0.004		0.046		0.569
H-pol 45°		0.523	0.641	−0.009	0.000	0.044	0.049	
L- and X-band	572	−0.195		0.056		0.051		0.649
Dual-pol 45°		−0.272	−0.115	0.051	0.060	0.048	0.054	
C- and X-band	417	0.338		0.032		0.089		−0.121
H-pol 45°		0.251	0.421	0.024	0.041	0.083	0.095	
C- and X-band	562	−0.069		0.125		0.076		0.823
Dual-pol 45°		−0.151	0.014	0.119	0.131	0.072	0.081	
L-, C- and X-band	509	0.633		−0.019		0.034		0.407
H-pol 45°		0.578	0.682	−0.022	−0.016	0.032	0.036	
L-, C- and X-band	572	−0.316		0.042		0.058		0.600
Dual-pol 45°		−0.388	−0.240	0.038	0.047	0.055	0.062	

From the time series comparison, the soil moisture observed/retrieved by the radiometer all shows steeper slopes (wet faster and dry faster) during the dry-down periods compared to the in situ measurements at 2.5 cm. This result is more significant when the radiometer captures a precipitation/irrigation event. It is reasonable that the radiometer may "see" an even shallower layer of soil than 2.5 cm. When rainfall or irrigation occurs, the top layer of soil immediately gets wet, while the soil moisture sensor at the lower layer shows a drier value. Compared to dual-channel retrievals, the soil moisture retrieved with all incidence angles, from 40° to 65° (with an interval of 2.5°, H-pol only), shows intermediate performance (dry bias of −0.012 cm^3/cm^3 and ubRMSD of 0.03 cm^3/cm^3), as all collaborative information is accounted for by the cost function.

The vegetation tau retrievals at the core channel (incidence angles at 40°, 45° and 50°) are compared to in situ vegetation water content measurements. It can be seen that the retrieved vegetation tau values increase as the incidence angle of the core channel increases. It was previously remarked that higher soil moisture is retrieved for higher incidence angles, possibly due to sky contamination in the observed brightness temperatures. Thus, it is reasonable that a lower soil contribution (higher soil moisture) leads to a greater vegetation contribution (higher vegetation tau) to the total brightness temperature signal. In addition, this result may indicate that the assumption that vegetation signals are incidence-angle independent ($C_P = 1$) is not valid for corn fields due to structural effects, which could be particularly significant for the small spatial scales observed by ground-based radiometers compared to satellites providing large-scale averages. The vegetation tau retrievals present reasonable variation that follows the measured/fitted vegetation water content and reaches a maximum at the end of the experiment (approximately August 27, 2017). It is very interesting that the correlation between the retrieved vegetation tau values and the measured vegetation water content increases as the incidence angle increases and reaches a maximum value of 0.861 for dual-angular retrievals from 50° and 65° (H-pol only). In addition, the retrieval of vegetation tau is very stable and does not follow the same variation as that observed in the soil moisture, indicating a successful separation of the soil and vegetation contributions.

The soil moisture and vegetation tau values were then retrieved (Fig. 12) based on the multi-frequency approach with single H-pol or dual-pol observations in the corn field. The analysis was only conducted at an incidence angle of 45°, which is considered to be less affected by radiation from the truck and sky than other incidence angles (Zhao et al., 2020b). There are four combinations, including the L- and C-bands, L- and X-bands, C- and X-bands, and L-, C- and X-bands, and the combination with the L- and C-bands (H-pol only) achieves the best performance (bias of −0.024 cm^3/cm^3 and ubRMSD of 0.028 cm^3/cm^3), which is comparable to that of the dual-angular combination of 40° and 55°. However, the retrieval performance of the soil moisture generally degrades as the frequency increases, especially when the measured vegetation water content is greater than 3 kg/m^2. It can be imagined that the sensitivity to soil moisture degrades as the wavelength becomes shorter due to the weakening penetration ability and increased scattering inside the vegetation. Therefore, the significance of the soil moisture and vegetation conditions "seen" by the radiometer are not the same among different frequencies. Hence, in the implementation of the MCCA, the soil moisture and vegetation tau are retrieved only for the single core channel, and information from other collaborative channels is only used to help find the solution. These results seem to contrast with our previous finding that the soil moisture explains a large part of the difference in the brightness temperatures between the C- band and X-band. It should be noted that the MCCA utilizes the brightness temperature at the core channel to predict those of the other channels and does not directly use the difference between two channels. This result also indicates that a consistent setting may not work with all channel combinations, as the

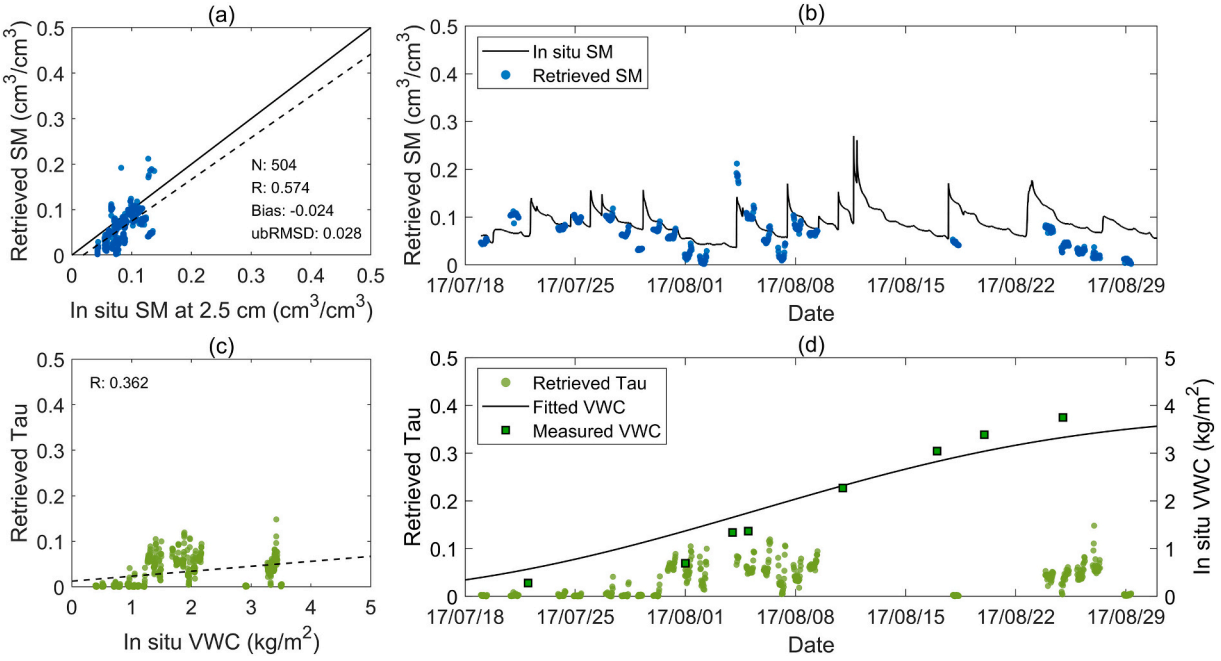

Fig. 9. Soil moisture (a, b) and vegetation tau (c, d) retrievals with L-band H-pol brightness temperatures at 40° and 55° in the corn field. Blue dots show the retrieved soil moisture, and green dots show the retrieved vegetation tau values. Green squares show the in situ measured vegetation water content with a fitted function as a solid line. (For interpretation of the references to colour in this figure legend, the reader is referred to the web version of this article.)

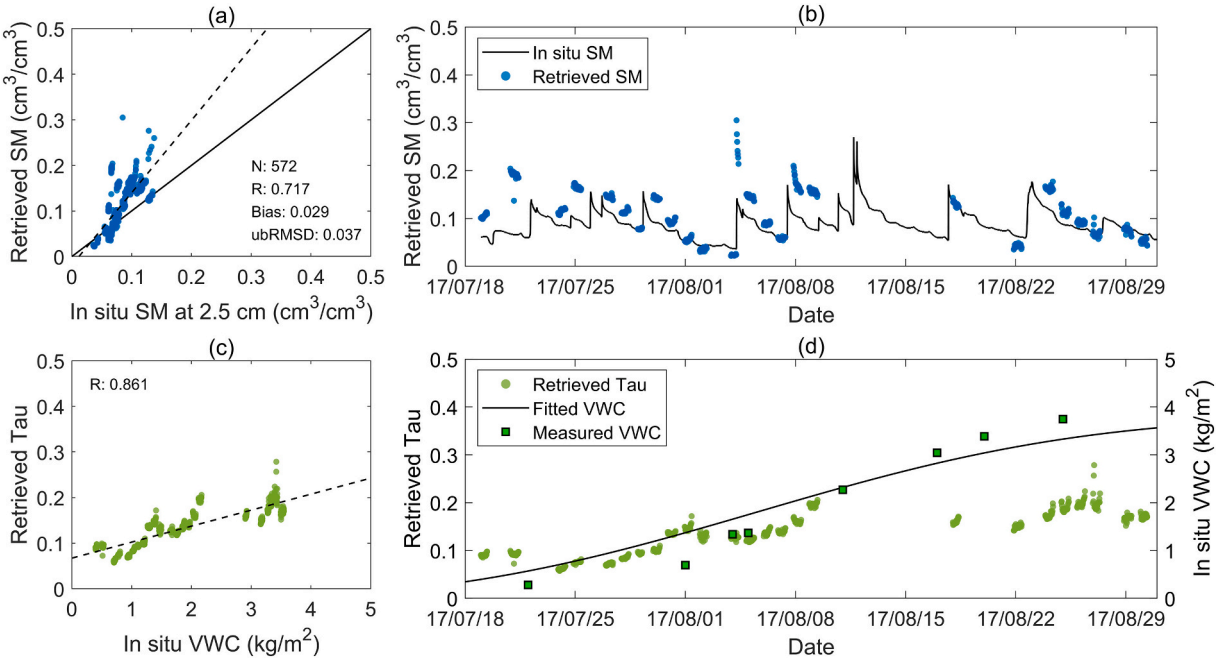

Fig. 10. Soil moisture (a, b) and vegetation tau (c, d) retrievals with L-band H-pol brightness temperatures at 50° and 65° in the corn field. Blue dots show the retrieved soil moisture, and green dots show the retrieved vegetation tau values. Green squares show the in situ measured vegetation water content with a fitted function as a solid line. (For interpretation of the references to colour in this figure legend, the reader is referred to the web version of this article.)

assumption of Eq. (19) can becomes weak. Similarly, for the H-pol-only retrievals, the soil moisture estimated with all three frequencies had an intermediate performance (dry bias of -0.019 cm^3/cm^3 and ubRMSD of 0.034 cm^3/cm^3) with more retrievals.

The results obtained for the corn field revealed that both soil moisture and vegetation tau could be estimated based on the multi-angular or multi-frequency approach of the MCCA. Soil moisture retrievals obtained with multi-frequency observations generally show less robustness and slightly lower performances compared to retrievals obtained with multi-angular observations, although multi-frequency observations contain more information, as found above. It should be noted that the retrievals obtained with dual-pol observations are not derived purely from multi-angular or multi-frequency information, as polarization information is also incorporated, and this incorporation generally allows a larger number of retrievals and achieves worse performances compared to those of the single H-pol retrievals in our case. This may indicate that

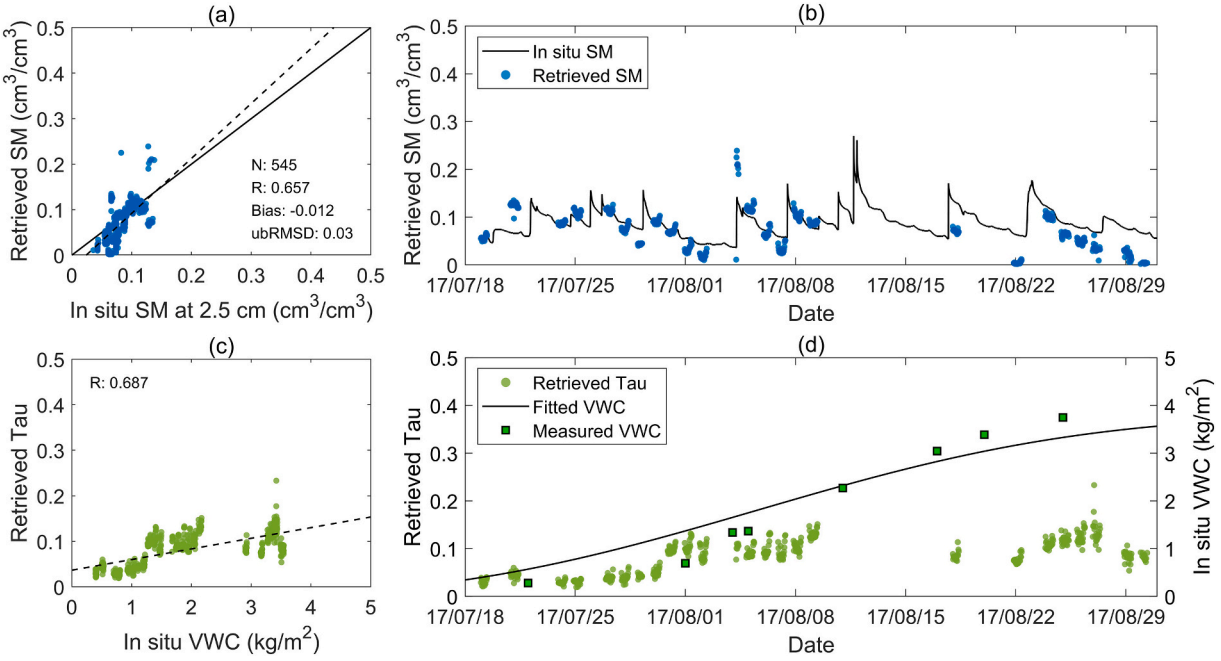

Fig. 11. Soil moisture (a, b) and vegetation tau (c, d) retrievals with L-band H-pol brightness temperatures from 40° to 65° in the corn field. Blue dots show the retrieved soil moisture, and green dots show the retrieved vegetation tau values. Green squares show the in situ measured vegetation water content with a fitted function as a solid line. (For interpretation of the references to colour in this figure legend, the reader is referred to the web version of this article.)

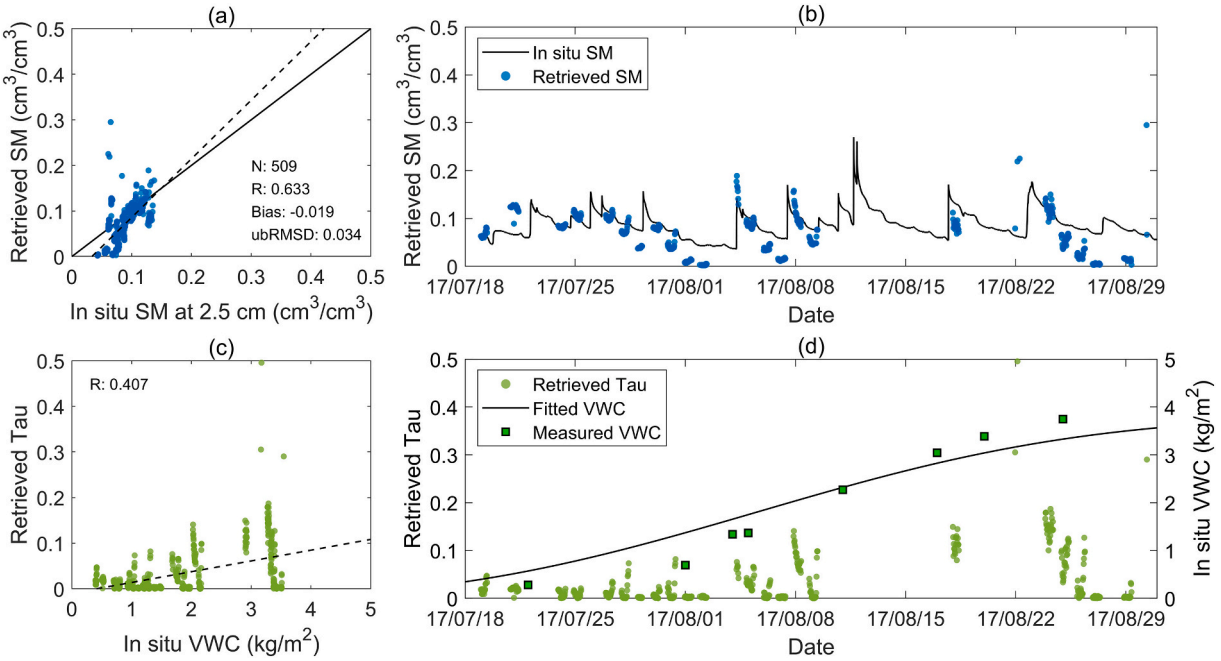

Fig. 12. Soil moisture (a, b) and vegetation tau (c, d) retrievals with L-, C- and X-band H-pol brightness temperatures at 45° in the corn field. Blue dots show the retrieved soil moisture, and green dots show the retrieved vegetation tau values. Green squares show the in situ measured vegetation water content with a fitted function as a solid line. (For interpretation of the references to colour in this figure legend, the reader is referred to the web version of this article.)

the "isotropic" assumption cannot fully account for the realistic structures of corn fields. The multi-angular approach of the MCCA could be used to yield comparable soil moisture results (half hourly observations with 572 records, ubRMSD: 0.028 to 0.037 cm^3/cm^3) with those of other algorithms used in a previous study (Zhao et al., 2020b), in which it was found that all algorithms could achieve ubRMSD values within the mission target (hourly observations with 286 records, SCA-V: 0.017 to 0.033 cm^3/cm^3; SCA—H: 0.025 to 0.032 cm^3/cm^3; DCA: 0.025 to 0.031 cm^3/cm^3; LPRM: 0.021 to 0.032 cm^3/cm^3). The vegetation tau values retrieved by the MCCA normally show larger fluctuations than those of the soil moisture retrievals because soil moisture is the most sensitive parameter in passive microwave remote sensing of landscapes at L-, C- and X-bands. During the retrieval with a given brightness temperature, a small proportion of changes in the soil moisture corresponds to a larger proportion of changes in the vegetation tau value. This is true for all types of retrieval algorithms, and the application of a moving-average

filter to the vegetation tau is recommended before its scientific use (Konings et al., 2017; Vittucci et al., 2019). Therefore, as seen from Fig. 10 (dual-angular retrievals), Fig. 11 (multi-angular retrievals) and Fig. 12 (multi-frequency retrievals), the retrieval performance of soil moisture does not change much (R from 0.633 to 0.717, ubRMSD from 0.030 cm^3/cm^3 to 0.037 cm^3/cm^3), but the retrieved vegetation tau could become significantly worse in terms of its correlation coefficient with the vegetation water content (R from 0.407 to 0.861). However, the vegetation tau retrievals obtained from the MCCA are good enough compared to those obtained in a previous study (Zhao et al., 2020b) conducted from the same dataset. The best correlation coefficient between the vegetation tau and water content is 0.861 (572 records) from the MCCA, while the best correlation coefficients obtained from the DCA and LPRM algorithms are 0.73 and 0.71 (286 records), respectively. Notably, the vegetation tau retrievals obtained with the multi-frequency approach of the MCCA present a dependence on the retrieved soil moisture (high vegetation tau accompanied by high soil moisture), indicating that the soil and vegetation contributions may not be well-separated.

4.4. Retrievals in the grass field

The MCCA was then applied for soil moisture and vegetation tau retrievals from the grass field. As the vegetation did not vary greatly throughout the experimental area (the vegetation water content ranges from 0.1 kg/m^2 to 0.5 kg/m^2 without any obvious trend), only soil moisture results are presented here, with the performance metrics of R, bias, and ubRMSD with 95% confidence intervals shown in Table 4. No significant difference is expected between different dual-angular combinations since the vegetation effects in the grass field are small. All the dual-angular retrievals of soil moisture present a dry bias when compared with in situ measurements taken at a depth of 3 cm. The soil moisture retrievals obtained from observations at 50° and 65° perform best, with a best bias value of −0.037 cm^3/cm^3 for dual-pol and a minimum ubRMSD of 0.026 cm^3/cm^3 for single H-pol. Similar to the corn field, the estimated soil moisture values increase as the incidence angle increases for the single H-pol case. One of the reasons for this result is that brightness temperatures at larger incidence angles might be affected by radiation from the sky, as mentioned above. However, the correction of side-lobe artefacts is a complex process that is out of the scope of this study. The soil moisture retrievals obtained with multi-angular observations (40° to 65°, H-pol only) have a similar performance (bias of −0.099 cm^3/cm^3, ubRMSD of 0.034 cm^3/cm^3 and R of 0.962) with that of the dual-angular retrievals, as shown in Fig. 13a and b.

Except for the C- and X-band combination, there are no significant differences observed in the soil moisture retrieval performances when using the L-band as the core channel. The combination with the L- and C-bands (single H-pol) achieves the best performance (bias of −0.059 cm^3/cm^3 and ubRMSD of 0.018 cm^3/cm^3), while the multi-frequency approach with the L-, C- and X-bands (single H-pol) has an intermediate performance (bias of −0.065 cm^3/cm^3 and ubRMSD of 0.018 cm^3/cm^3), as shown in Figs. 13c and 15d. For the multi-frequency approach, the performance of the soil moisture retrieval is slightly degraded by adding polarization information. All the soil moisture retrievals obtained from the multi-frequency observations at 45° also show dry biases.

As mentioned above, the soil moisture observed by the radiometer might be more correlated to a shallower layer than to the depth of 2.5 cm in the corn field. This is found from the shape of the soil moisture estimation during the dry-down periods. However, no precipitation events were captured by the radiometer in the grass field. The dry bias in the grass field is more obvious in both the multi-angular and multi-frequency approaches when compared with the soil moisture measurements obtained at a depth of 3 cm. In Fig. 14, soil moisture retrievals are compared with the average soil moisture values at 3 cm and 1 cm.

Table 4
Retrieval performances in the grass field. [X_l X_u] rows are the 95% confidence intervals of the X (being R, Bias, ubRMSD) estimates.

Configuration	Number	R		Bias		ubRMSD	
		R_l	R_u	Bias_l	Bias_u	ubRMSD_l	ubRMSD_u
L-band H-pol	536	0.965		−0.099		0.033	
40° and 55°		0.959	0.970	−0.102	−0.096	0.031	0.035
L-band Dual-pol	536	0.912		−0.088		0.033	
40° and 55°		0.897	0.925	−0.091	−0.085	0.031	0.035
L-band H-pol	536	0.966		−0.093		0.029	
45° and 60°		0.960	0.972	−0.096	−0.091	0.028	0.031
L-band Dual-pol	536	0.923		−0.070		0.027	
45° and 60°		0.909	0.935	−0.072	−0.068	0.025	0.028
L-band H-pol	536	0.973		−0.088		0.026	
50° and 65°		0.968	0.977	−0.090	−0.085	0.025	0.028
L-band Dual-pol	536	0.910		−0.037		0.033	
50° and 65°		0.894	0.924	−0.040	−0.035	0.031	0.035
L-band H-pol	536	0.962		−0.099		0.034	
40° to 65°		0.956	0.968	−0.101	−0.096	0.032	0.036
L-band Dual-pol	536	0.951		−0.097		0.034	
40° to 65°		0.942	0.959	−0.100	−0.094	0.032	0.037
L- and C-band	536	0.964		−0.059		0.018	
H-pol 45°		0.958	0.970	−0.061	−0.058	0.017	0.019
L- and C-band	536	0.954		−0.059		0.020	
Dual-pol 45°		0.945	0.961	−0.061	−0.057	0.019	0.021
L- and X-band	536	0.966		−0.071		0.020	
H-pol 45°		0.960	0.971	−0.073	−0.069	0.018	0.021
L- and X-band	536	0.945		−0.071		0.023	
Dual-pol 45°		0.936	0.954	−0.073	−0.069	0.022	0.025
C- and X-band	536	0.310		−0.138		0.064	
H-pol 45°		0.231	0.384	−0.144	−0.133	0.060	0.068
C- and X-band	536	0.047		−0.115		0.085	
Dual-pol 45°		−0.038	0.131	−0.122	−0.107	0.080	0.091
L-, C- and X-band	536	0.965		−0.065		0.018	
H-pol 45°		0.958	0.970	−0.066	−0.063	0.017	0.019
L-, C- and X-band	536	0.956		−0.067		0.020	
Dual-pol 45°		0.948	0.963	−0.068	−0.065	0.019	0.022

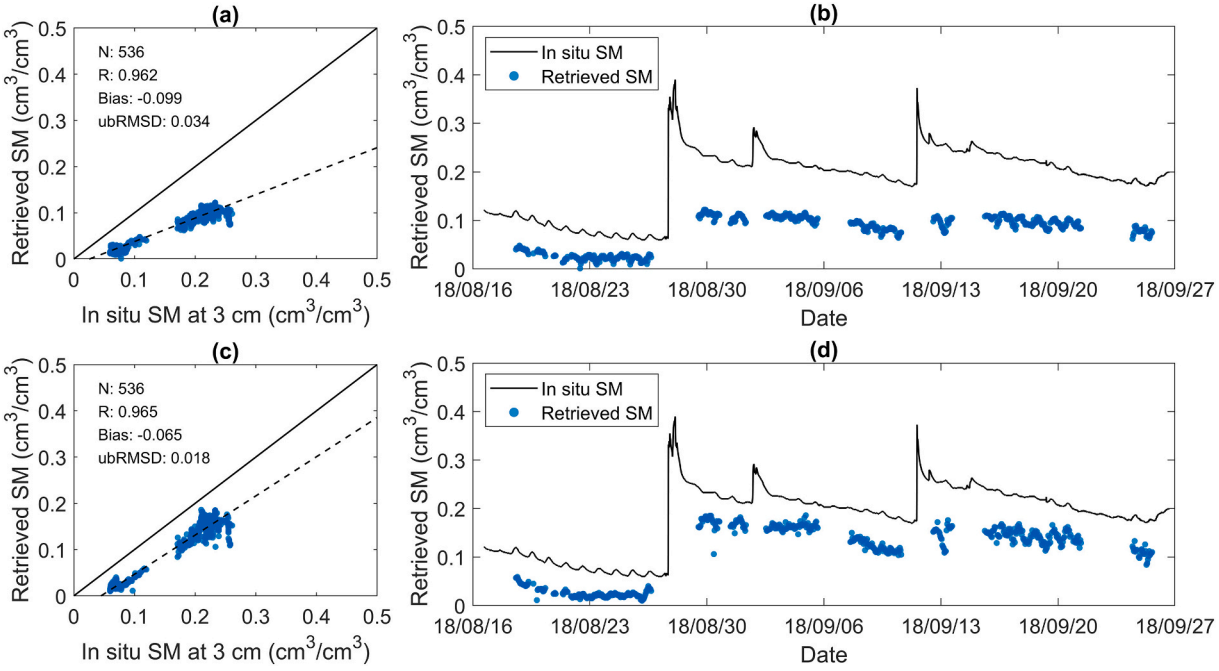

Fig. 13. Soil moisture retrievals in the grass field. (a) and (b) show a scatterplot and a time-series plot, respectively, of in situ measured soil moisture versus soil moisture retrievals obtained by using the L-band (H-pol) brightness temperatures from 40° to 65°. (c) and (d) show a scatterplot and a time-series plot, respectively, of in situ measured soil moisture versus soil moisture retrievals obtained by using L-, C- and X-band (H-pol) brightness temperatures at 45°.

Although the measurements taken at 1 cm might be unreliable, as the probe may "see" the air due to the 715-mL measurement volume of the 5TM sensor, the retrieved soil moisture values match the average values, especially those obtained with the multi-frequency approach (single H-pol, bias of 0.0 cm^3/cm^3 and ubRMSD of 0.017 cm^3/cm^3). This further confirms that the microwave remotely sensed soil moisture might be more sensitive to a shallower soil layer than 3 cm, at least in the experimental areas of this study.

It should be noted that all data are retrieved in the grass field, with a total number of 536. This is attributed to the very low vegetation effects (vegetation water content less than 0.5 kg/m^2). In contrast to the corn field (maximum vegetation water content of 3.7 kg/m^2), in the grass field, the multi-frequency approach generally performs better than the multi-angular approach, with lower ubRMSD values, with the exception of the C- and X-band combination. This can be expected because the weakest assumption, that of the dependence of vegetation tau on frequency, cannot play a role when the vegetation contribution is very low.

4.5. Discussions on increasing observation channels

Under normal circumstances, it is believed that increasing the number of observation channels is beneficial to the retrieval of surface parameters because the *DoI* obtained by the retrieval algorithm will increase. The effects of an increasing number of observation channels are further discussed using soil moisture retrievals obtained by the MCCA in the corn field. Fig. 15 presents the variations in the performances of soil moisture retrievals resulting from increasing the number of incidence angles with both single H-pol and dual-pol options, e.g., $\{Tb^{total}_{H,\,40^\circ,\,L}, Tb^{total}_{H,\,42.5^\circ,\,L}\}$, $\{Tb^{total}_{H,\,40^\circ,\,L}, Tb^{total}_{H,\,42.5^\circ,\,L}, Tb^{total}_{H,\,45^\circ,\,L}\}$, … $\{Tb_{H,\,40^\circ,\,L}{}^{total}, Tb^{total}_{H,\,42.5^\circ,\,L}, \ldots Tb^{total}_{H,\,65^\circ,\,L}\}$.

For the single H-pol retrieval (Fig. 15a), all the statistical metrics (R, bias, and ubRMSD) follow a "U" shape. The bias and R values reach maximums (bias: −0.012 cm^3/cm^3, R: 0.657) when all 11 angles are used. The ubRMSD continues to decrease as the number of angles increases and reaches its minimum value (0.028 cm^3/cm^3) when 10 angles are used. The ubRMSD is slightly increased to 0.03 cm^3/cm^3 when using all the angles. For the dual-pol implementation (Fig. 15b), with an increasing number of angles, R generally increases (to a maximum value of 0.66), while ubRMSD generally decreases and reaches its minimum value (0.03 cm^3/cm^3) when 10 angles are used. The bias first increases and then decreases to a maximum value (−0.009 cm^3/cm^3) closest to 0 as the number of angles increases. Notably, the soil moisture retrievals obtained from the dual-pol implementation could be worse than those obtained from the single H-pol implementation, because the dependence of vegetation parameters on polarization (e.g., single scattering albedo and polarization dependent parameter, C_P) are not considered in this study. Generally, our results affirm that the soil moisture retrievals tend to become more robust as the number of included observation angles increase. However, it has to be clarified that there is no guarantee that the best results will be obtained by using the most angles (channels). This is because the current soil moisture algorithms (including the MCCA used in this study) are mainly based on the simple omega-tau model. Some assumptions are made in forward models and retrieval algorithms, especially including the dependence of vegetation on the polarization, incidence angle and frequency. When more observation channels are added, the probability that the model outputs will not match the observations could increase, which would affect the process of minimizing the cost function. In addition, the decrease in the signal-to-noise ratio caused by the use of an increasing number of observation channels may also have negative impacts on the retrieval performance.

5. Summary and conclusions

In this study, SMELR ground-based measurements of microwave radiometry over corn and grass fields are used to explore multi-angular and multi-frequency approaches for the retrieval of soil moisture and vegetation tau. The independent information contained within the passive microwave observations was first investigated using the concept of the *DoI*, based on a dataset collected in a corn field. Then, the polarization, frequency, and incidence-angle information, represented by the NPDI, NFDI and NADI, respectively, was decomposed into contributions from soil moisture and vegetation water content through the proportion of the explained variance, η^2. Finally, a new algorithm, the MCCA, was developed to utilize multi-channel observations as

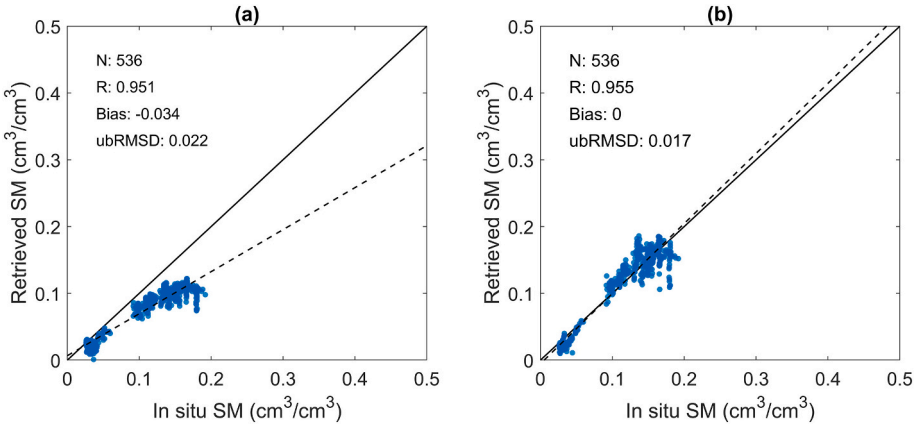

Fig. 14. Soil moisture retrievals versus average soil moisture between 1 cm and 3 cm in the grass field. (a) Scatterplot of retrievals obtained with L-band (H-pol) brightness temperatures from 40° to 65°, (b) scatterplot of retrievals obtained with L-, C- and X-band (H-pol) brightness temperatures at 45°.

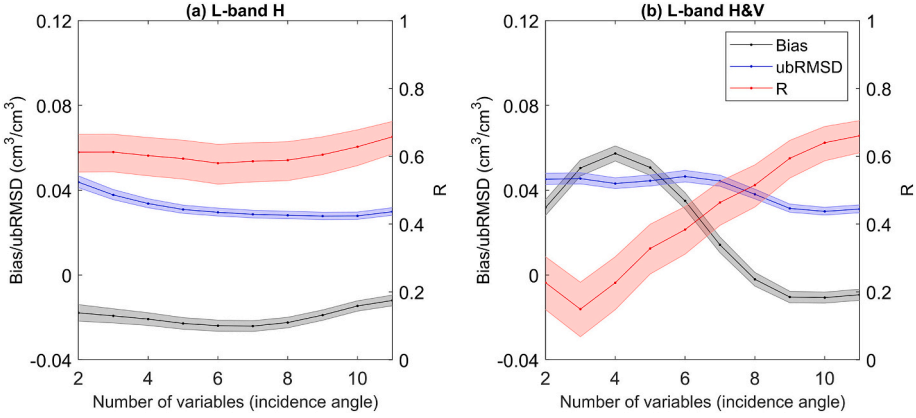

Fig. 15. Variations in soil moisture retrieval performance in the corn field with the number of variables in terms of the incidence angle. The 2 angles refer to as {40°, 42.5°}, and the 11 angles refer to as {40°, 42.5°, … 65°}. The black, blue, and red dots are calculated performance metrics, and their confidence intervals are presented with shaded colour bars. (For interpretation of the references to colour in this figure legend, the reader is referred to the web version of this article.)

restrictions with which to select the candidate parameters to be retrieved. The retrieval performance for soil moisture and vegetation tau was analyzed by comparing with in situ measurements. The main conclusions are summarized below.

Compared to the C- and X-bands, the L-band contains more independent information (larger *DoI*) with the given configuration of multi-angular polarized observations in the crop field. The *DoI* reaches its maximum around Brewster's angle with the given configuration of multi-frequency polarized observations. It is found that the *DoI* increases linearly with the number of variables/channels in terms of the incidence angle and frequency. With the same number of observation channels, multi-frequency observations contain more independent information with slightly larger *DoI* compared to multi-angular observations. However, the increase in *DoI* that occurs with multi-frequency observations is mainly attributed to the dependence of vegetation signatures on frequency, which may bring about more difficulties to soil moisture retrievals when the vegetation effects are significant; this is affirmed later in the study using MCCA retrievals. This result also indicates that the *DoI* may not be a complete picture of how many parameters can be estimated and should be paired with the signal-to-noise ratio. On the other hand, the independent information contained within microwave observations can be condensed as brightness temperature difference indices. The polarization difference in terms of the NPDI is sensitive to both the soil moisture and vegetation water content, especially at L-band, in which there is a comparable proportion of explained variance. The frequency differences in terms of the NFDI, especially at adjacent frequencies (L- & C-bands, C- & X-bands), are only sensitive to soil moisture, with a large proportion of explained variance. Vegetation water content explains most of the variance in the angular differences in terms of the NADI. These results suggest that the NFDI and NADI could be utilized in the retrieval of soil moisture (e.g., CIMR) and vegetation tau values (e.g., SMOS), respectively.

The main advantages of the newly developed MCCA are summarized as follows:

i. Using an analytical equation of brightness temperatures at any two channels as conditional restrictions, the MCCA allows the use of any two or more channels of brightness temperatures for retrieval.
ii. The MCCA requires no priori information on vegetation with a main assumption regarding how the vegetation tau varies across different polarizations, incidence angles, and wavelengths/frequencies.
iii. The implementation of the MCCA with paired/grouped candidate parameters could avoid obtaining multiple minima during the minimization process.

With the experimental data collected in the corn and grass fields, the MCCA was found to be able to retrieve both soil moisture and vegetation tau simultaneously. For the corn field, where the maximum vegetation water content is 3.75 kg/m^2, the soil moisture retrieval with the multi-angular observations performs (bias from −0.024 cm^3/cm^3 to 0.039

cm^3/cm^3, ubRMSD from 0.028 cm^3/cm^3 to 0.037 cm^3/cm^3) generally better than does the retrieval with the multi-frequency observations (bias from −0.024 cm^3/cm^3 to 0.056 cm^3/cm^3, ubRMSD from 0.028 cm^3/cm^3 to 0.089 cm^3/cm^3). This affirms that the increase in independent information that occurs with multi-frequency observations may bring about more unknowns or higher uncertainty in the vegetation tau, which make retrieval more challenging. For the grass field, where the vegetation water content is less than 0.5 kg/m^2, the retrievals obtained with the multi-frequency observations perform better (bias from −0.071 cm^3/cm^3 to −0.059 cm^3/cm^3, ubRMSD from 0.018 cm^3/cm^3 to 0.023 cm^3/cm^3) than those obtained with the multi-angular observations (bias from −0.099 cm^3/cm^3 to −0.037 cm^3/cm^3, ubRMSD from 0.026 cm^3/cm^3 to 0.034 cm^3/cm^3), with the exception of the C-band & X-band combination. This is consistent with the finding that soil moisture explains most of the variance in frequency differences in brightness temperature if the vegetation tau does not differ greatly across wavelengths. It is further found that soil moisture retrievals are not improved by incorporating dual-pol observations, which indicates that the assumption of "isotropic" vegetation needs to be refined to consider polarization dependence. Our results also show that the soil moisture retrieved by microwave radiometry may show a sharper dry-down trend compared with in situ measurements and can lead to biased soil moisture retrievals, which may indicate that the passive microwave remotely sensed soil moisture may be more sensitive to a layer shallower than 3 cm. However, this needs further investigation at the global scale with much larger footprints at tens of kilometer. The results of the MCCA demonstrate that high-performance metrics compared with in situ measurements can be achieved for both soil moisture and vegetation tau retrievals, and only when the soil moisture and vegetation tau are not closely related the retrievals might be considered successful, indicating a good separation of the soil and vegetation contributions. Further discussions affirm that the soil moisture retrievals tend to be more robust when a greater number of observation channels are incorporated, but the retrieval performance may be limited by the increased probability that the model estimations will not match the observations.

The main limitation of this study is that the analyses and retrievals are only conducted with ground-based experimental data of two typical land cover types. It is assumed that the footprints and the whole experimental field are uniform in this study, with the fraction of vegetation coverage equal to 100%, while multi-angular or multi-frequency signals are emitted from different objects on the ground. Further investigation with satellite observations is needed to consider heterogeneity. Nevertheless, it can be inferred that the multi-angular payload configuration at the optimal L-band (e.g., SMOS) should be the best choice for the purpose of soil moisture retrievals since the vegetation tau is relatively uniform across the incidence angle and most land surfaces are covered by vegetation. The payload configuration with multi-frequency abilities not only provides the ability for soil moisture mapping but also provides a chance to explore vegetation properties across wavelengths. The optimal selection of the incidence angle should be slightly less than Brewster's angle (e.g., 40° for the SMAP), obtained by considering both the *DoI* contamination and the penetrating ability. In addition, a multi-frequency satellite mission (e.g., WCOM, CIMR) can be used for the estimation of other parameters related to the water cycle for the fulfilment of even broader scientific requirements. Further, concerning the RFI issue, the C-band is not protected and made AMSR-E/2 soil moisture products to depend mainly on X-band, which is less influenced by the RFI in certain regions. SMOS and SMAP are supposedly operating on a protected band, but many contaminations are still reported in some regions. Active filtering techniques, such as sub-band and sub-time sampling for SMAP, can considerably reduce the RFI impacts at the cost of increased noise levels. Therefore, a satellite mission with both capabilities at multiple incidence angles (privileged range of incidence angles from 30° to 50°, Zhao et al., 2020b) and multiple frequencies (e.g., L-, X-, and Ka-bands, L-, X-, K-, and Ka-bands), which can be achieved by an integrated design of several 2-dimensional synthetic aperture radiometers, would greatly improve the quality of retrieved land parameters and thus promote the application of remote sensing in Earth system studies.

Declaration of Competing Interest

The authors declare that they have no known competing financial interests or personal relationships that could have appeared to influence the work reported in this paper.

Acknowledgments

This study was jointly supported by the Second Tibetan Plateau Scientific Expedition and Research Program (No. 2019QZKK0206), the National Natural Science Foundation of China (No. 41671355) and the Strategic Priority Research Program of Chinese Academy of Sciences (No. XDA20100300).

Appendix A. Supplementary material

Supplementary material to this article can be found online at https://doi.org/10.1016/j.rse.2021.112321.

References

Al Bitar, A., Mialon, A., Kerr, Y.H., Cabot, F., Richaume, P., Jacquette, E., Quesney, A., Mahmoodi, A., Tarot, S., Parrens, M., Al-yaari, A., 2017. The global SMOS level 3 daily soil moisture and brightness temperature maps. Earth Syst. Sci. Data 293–315. https://doi.org/10.5194/essd-9-293-2017.

Al-Yaari, A., Wigneron, J.-P., Kerr, Y., Rodriguez-Fernandez, N., O'Neill, P.E., Jackson, T. J., De Lannoy, G.J.M., Al Bitar, A., Mialon, A., Richaume, P., Walker, J.P., Mahmoodi, A., Yueh, S., 2017. Evaluating soil moisture retrievals from ESA's SMOS and NASA's SMAP brightness temperature datasets. Remote Sens. Environ. 193, 257–273. https://doi.org/10.1016/j.rse.2017.03.010.

Al-Yaari, A., Wigneron, J.-P., Dorigo, W., Colliander, A., Pellarin, T., Hahn, S., Mialon, A., Richaume, P., Fernandez-Moran, R., Fan, L., Kerr, Y.H., De Lannoy, G., 2019. Assessment and inter-comparison of recently developed/reprocessed microwave satellite soil moisture products using ISMN ground-based measurements. Remote Sens. Environ. 224, 289–303. https://doi.org/10.1016/j.rse.2019.02.008.

Baur, M.J., Jagdhuber, T., Feldman, A.F., Akbar, R., Entekhabi, D., 2019. Estimation of relative canopy absorption and scattering at L-, C- and X-bands. Remote Sens. Environ. 233, 111384. https://doi.org/10.1016/j.rse.2019.111384.

Becker, F., Choudhury, B.J., 1988. Relative sensitivity of normalized difference vegetation index (NDVI) and microwave polarization difference index (MPDI) for vegetation and desertification monitoring. Remote Sens. Environ. 24, 297–311. https://doi.org/10.1016/0034-4257(88)90031-4.

Bindlish, R., Jackson, T., Zhao, T., 2011. A MODIS-based vegetation index climatology. Remote Sens. Model. Ecosyst. Sustain. VIII 8156, 815603. https://doi.org/10.1117/12.890311.

Brandt, M., Wigneron, J.P., Chave, J., Tagesson, T., Penuelas, J., Ciais, P., Rasmussen, K., Tian, F., Mbow, C., Al-Yaari, A., Rodriguez-Fernandez, N., Schurgers, G., Zhang, W., Chang, J., Kerr, Y., Verger, A., Tucker, C., Mialon, A., Rasmussen, L.V., Fan, L., Fensholt, R., 2018. Satellite passive microwaves reveal recent climate-induced carbon losses in African drylands. Nat. Ecol. Evol. 2, 827–835. https://doi.org/10.1038/s41559-018-0530-6.

Brocca, L., Ciabatta, L., Massari, C., Camici, S., Tarpanelli, A., 2017. Soil moisture for hydrological applications: open questions and new opportunities. Water 9, 140. https://doi.org/10.3390/w9020140.

Chan, S.K., Bindlish, R., O'Neill, P.E., Njoku, E., Jackson, T., Colliander, A., Chen, F., Burgin, M., Dunbar, S., Piepmeier, J., Yueh, S., Entekhabi, D., Cosh, M.H., Caldwell, T., Walker, J., Wu, X., Berg, A., Rowlandson, T., Pacheco, A., McNairn, H., Thibeault, M., Martinez-Fernandez, J., Gonzalez-Zamora, A., Seyfried, M., Bosch, D., Starks, P., Goodrich, D., Prueger, J., Palecki, M., Small, E.E., Zreda, M., Calvet, J.C., Crow, W.T., Kerr, Y., 2016. Assessment of the SMAP passive soil moisture product. IEEE Trans. Geosci. Remote Sens. 54, 4994–5007. https://doi.org/10.1109/TGRS.2016.2561938.

Chan, S.K., Bindlish, R., Neill, P.O., Jackson, T., Njoku, E., Dunbar, S., Chaubell, J., Piepmeier, J., Yueh, S., Entekhabi, D., Colliander, A., Chen, F., Cosh, M.H., Caldwell, T., Walker, J., Berg, A., Mcnairn, H., Thibeault, M., Martínez-fernández, J., Uldall, F., Seyfried, M., Bosch, D., Starks, P., Holi, C., Prueger, J., Van Der Velde, R., Asanuma, J., Palecki, M., Small, E.E., Zreda, M., Calvet, J., Crow, W.T., Kerr, Y., 2018. Development and assessment of the SMAP enhanced passive soil moisture product. Remote Sens. Environ. 204, 931–941. https://doi.org/10.1016/j.rse.2017.08.025.

Chaubell, M.J., Asanuma, J., Berg, A.A., Bosch, D.D., Caldwell, T., Cosh, M.H., Collins, C. H., Martinez-Fernandez, J., Seyfried, M., Starks, P.J., Su, Z., Yueh, S.H., Thibeault, M., Walker, J., Dunbar, R.S., Colliander, A., Chen, F., Chan, S.K., Entekhabi, D., Bindlish, R., O'Neill, P.E., 2020. Improved SMAP dual-channel

algorithm for the retrieval of soil moisture. IEEE Trans. Geosci. Remote Sens. 1–12. https://doi.org/10.1109/tgrs.2019.2959239.
Chen, F., Crow, W.T., Bindlish, R., Colliander, A., Burgin, M.S., Asanuma, J., Aida, K., 2018. Global-scale evaluation of SMAP, SMOS and ASCAT soil moisture products using triple collocation. Remote Sens. Environ. 214, 1–13. https://doi.org/10.1016/j.rse.2018.05.008.
Choudhury, B.J., Schmugge, T.J., Mo, T., 1982. Parameterization of effective soil temperature for microwave emission. J. Geophys. Res. 87, 1301–1304.
Colliander, A., Jackson, T.J., Bindlish, R., Chan, S., Das, N., Kim, S.B., Cosh, M.H., Dunbar, R.S., Dang, L., Pashaian, L., Asanuma, J., Aida, K., Berg, A., Rowlandson, T., Bosch, D., Caldwell, T., Caylor, K., Goodrich, D., Al Jassar, H., Lopez-Baeza, E., Martínez-Fernández, J., González-Zamora, A., Livingston, S., McNairn, H., Pacheco, A., Moghaddam, M., Montzka, C., Notarnicola, C., Niedrist, G., Pellarin, T., Prueger, J., Pulliainen, J., Rautiainen, K., Ramos, J., Seyfried, M., Starks, P., Su, Z., Zeng, Y., van der Velde, R., Thibeault, M., Dorigo, W., Vreugdenhil, M., Walker, J.P., Wu, X., Monerris, A., O'Neill, P.E., Entekhabi, D., Njoku, E.G., Yueh, S., 2017. Validation of SMAP surface soil moisture products with core validation sites. Remote Sens. Environ. 191, 215–231. https://doi.org/10.1016/j.rse.2017.01.021.
Corradini, C., 2014. Soil moisture in the development of hydrological processes and its determination at different spatial scales. J. Hydrol. 516, 1–5. https://doi.org/10.1016/j.jhydrol.2014.02.051.
Cosh, M.H., Jackson, T.J., Starks, P., Heathman, G., 2006. Temporal stability of surface soil moisture in the Little Washita River watershed and its applications in satellite soil moisture product validation. Remote Sens. Environ. 323, 168–177. https://doi.org/10.1016/j.jhydrol.2005.08.020.
Cui, Q., Shi, J., Du, J., Zhao, T., Xiong, C., 2015. An approach for monitoring global vegetation based on multiangular observations from SMOS. IEEE J. Sel. Top. Appl. Earth Obs. Remote Sens. 8, 604–616.
Cui, Q., Dong, X., Shi, J., Zhao, T., Xiong, C., 2016. An algorithm for retrieving soil moisture using L-band H-polarized multiangular brightness temperature data. IEEE Geosci. Remote Sens. Lett. 13, 1295–1299. https://doi.org/10.1109/LGRS.2016.2582518.
De Jeu, R.A.M., Owe, M., 2003. Further validation of a new methodology for surface moisture and vegetation optical depth retrieval. Int. J. Remote Sens. 24, 4559–4578. https://doi.org/10.1080/0143116031000095934.
De Jeu, R.A.M., Wagner, W., Holmes, T.R.H., Dolman, A.J., Giesen, N.C., Friesen, J., 2008. Global soil moisture patterns observed by space borne microwave radiometers and scatterometers. Surv. Geophys. 29, 399–420. https://doi.org/10.1007/s10712-008-9044-0.
Dorigo, W.A., Wagner, W., Hohensinn, R., Hahn, S., Paulik, C., Xaver, A., Gruber, A., Drusch, M., Mecklenburg, S., van Oevelen, P., Robock, A., Jackson, T., 2011. The international soil moisture network: a data hosting facility for global in situ soil moisture measurements. Hydrol. Earth Syst. Sci. 15, 1675–1698. https://doi.org/10.5194/hess-15-1675-2011.
Dorigo, W., Wagner, W., Albergel, C., Albrecht, F., Balsamo, G., Brocca, L., Chung, D., Ertl, M., Forkel, M., Gruber, A., Haas, E., Hamer, P.D., Hirschi, M., Ikonen, J., de Jeu, R., Kidd, R., Lahoz, W., Liu, Y.Y., Miralles, D., Mistelbauer, T., Nicolai-Shaw, N., Parinussa, R., Pratola, C., Reimer, C., van der Schalie, R., Seneviratne, S.I., Smolander, T., Lecomte, P., 2017. ESA CCI soil moisture for improved earth system understanding: state-of-the art and future directions. Remote Sens. Environ. 203, 185–215. https://doi.org/10.1016/j.rse.2017.07.001.
Ebtehaj, A., Bras, R.L., 2019. A physically constrained inversion for high-resolution passive microwave retrieval of soil moisture and vegetation water content in L-band. Remote Sens. Environ. 233, 111346. https://doi.org/10.1016/j.rse.2019.111346.
Entekhabi, D., Njoku, E.G., O'Neill, P.E., Kellogg, K.H., Crow, W.T., Edelstein, W.N., Entin, J.K., Goodman, S.D., Jackson, T.J., Johnson, J., Kimball, J., Piepmeier, J.R., Koster, R.D., Martin, N., McDonald, K.C., Moghaddam, M., Moran, S., Reichle, R., Shi, J.C., Spencer, M.W., Thurman, S.W., Tsang, L., Van Zyl, J., 2010. The soil moisture active passive (SMAP) mission. Proc. IEEE 98, 704–716. https://doi.org/10.1109/JPROC.2010.2043918.
Fan, L., Wigneron, J.-P., Ciais, P., Chave, J., Brandt, M., Fensholt, R., Saatchi, S.S., Bastos, A., Al-Yaari, A., Hufkens, K., Qin, Y., Xiao, X., Chen, C., Myneni, R.B., Fernandez-Moran, R., Mialon, A., Rodriguez-Fernandez, N.J., Kerr, Y., Tian, F., Peñuelas, J., 2019. Satellite-observed pantropical carbon dynamics. Nat. Plants 5, 944–951. https://doi.org/10.1038/s41477-019-0478-9.
Fernandez-Moran, R., Al-Yaari, A., Mialon, A., Mahmoodi, A., Al Bitar, A., De Lannoy, G., Rodriguez-Fernandez, N., Lopez-Baeza, E., Kerr, Y., Wigneron, J.P., 2017a. SMOS-IC: an alternative SMOS soil moisture and vegetation optical depth product. Remote Sens. 9 https://doi.org/10.3390/rs9050457.
Fernandez-Moran, R., Wigneron, J.-P., De Lannoy, G., Lopez-Baeza, E., Parrens, M., Mialon, A., Mahmoodi, A., Al-Yaari, A., Bircher, S., Al Bitar, A., Richaume, P., Kerr, Y., 2017b. A new calibration of the effective scattering albedo and soil roughness parameters in the SMOS SM retrieval algorithm. Int. J. Appl. Earth Obs. Geoinf. 62, 27–38. https://doi.org/10.1016/j.jag.2017.05.013.
Fujii, H., Koike, T., Imaoka, K., 2009. Improvement of the AMSR-E algorithm for soil moisture estimation by introducing a fractional vegetation coverage dataset derived from MODIS data. J. Remote Sens. Soc. Japan 29, 282–292.
Gao, L., Sadeghi, M., Ebtehaj, A., 2020. Microwave retrievals of soil moisture and vegetation optical depth with improved resolution using a combined constrained inversion algorithm: application for SMAP satellite. Remote Sens. Environ. 239, 111662. https://doi.org/10.1016/j.rse.2020.111662.
Gelman, A., 2005. Analysis of variance - why it is more important than ever. Ann. Stat. 33, 1–53. https://doi.org/10.1214/009053604000001048.
Gruber, A., De Lannoy, G., Albergel, C., Al-Yaari, A., Brocca, L., Calvet, J.C., Colliander, A., Cosh, M., Crow, W., Dorigo, W., Draper, C., Hirschi, M., Kerr, Y., Konings, A., Lahoz, W., McColl, K., Montzka, C., Muñoz-Sabater, J., Peng, J., Reichle, R., Richaume, P., Rüdiger, C., Scanlon, T., van der Schalie, R., Wigneron, J. P., Wagner, W., 2020. Validation practices for satellite soil moisture retrievals: what are (the) errors? Remote Sens. Environ. 244, 111806. https://doi.org/10.1016/j.rse.2020.111806.
Jackson, T.J., 1993. III. Measuring surface soil moisture using passive microwave remote sensing. Hydrol. Process. 7, 139–152.
Jackson, T.J., 1997. Soil moisture estimation using SSM/I satellite data over a grassland region. Water Resour. Res. 33, 1475–1484.
Jackson, T.J., Hsu, A.Y., Van de Griend, A., Eagleman, J.R., 2004. Skylab L-band microwave radiometer observations of soil moisture revisited. Int. J. Remote Sens. 25, 2585–2606. https://doi.org/10.1080/01431160310001647723.
Jackson, T.J., Hsu, A.Y., 2001. Soil moisture and TRMM microwave imager relationships in the southern Great Plains 1999 (SGP99) experiment. IEEE Trans. Geosci. Remote Sens. 39, 1632–1642.
Jackson, T.J., Schmugge, T.J., 1991. Vegetation effects on the microwave emission of soils. Remote Sens. Environ. 36, 203–212. https://doi.org/10.1016/0034-4257(91)90057-D.
Jackson, T.J., Cosh, M.H., Bindlish, R., Member, S., Starks, P.J., Bosch, D.D., Seyfried, M., Goodrich, D.C., Moran, M.S., Member, S., Du, J., 2010. Validation of advanced microwave scanning radiometer soil moisture products. IEEE Trans. Geosci. Remote Sens. 48, 4256–4272.
Jackson, T.J., Bindlish, R., Cosh, M.H., Zhao, T., Starks, P.J., Bosch, D.D., Seyfried, M., Moran, M.S., Goodrich, D.C., Kerr, Y.H., Leroux, D., 2012. Validation of soil moisture and ocean salinity (SMOS) soil moisture over watershed networks in the U.S. IEEE Trans. Geosci. Remote Sens. 50, 1530–1543.
Jones, L.A., Kimball, J.S., Podest, E., McDonald, K.C., Chan, S.K., Njoku, E.G., 2009. A method for deriving land surface moisture, vegetation optical depth, and open water fraction from AMSR-E. Int. Geosci. Remote Sens. Symp. 3, 916–919. https://doi.org/10.1109/IGARSS.2009.5417921.
Jones, M.O., Jones, L.A., Kimball, J.S., McDonald, K.C., 2011. Satellite passive microwave remote sensing for monitoring global land surface phenology. Remote Sens. Environ. 115, 1102–1114. https://doi.org/10.1016/j.rse.2010.12.015.
Jung, M., Reichstein, M., Ciais, P., Seneviratne, S.I., Sheffield, J., Goulden, M.L., Bonan, G., Cescatti, A., Chen, J., De Jeu, R., Dolman, A.J., Eugster, W., Gerten, D., Gianelle, D., Gobron, N., Heinke, J., Kimball, J., Law, B.E., Montagnani, L., Mu, Q., Mueller, B., Oleson, K., Papale, D., Richardson, A.D., Roupsard, O., Running, S., Tomelleri, E., Viovy, N., Weber, U., Williams, C., Wood, E., Zaehle, S., Zhang, K., 2010. Recent decline in the global land evapotranspiration trend due to limited moisture supply. Nature 467, 951–954. https://doi.org/10.1038/nature09396.
Kang, C.S., Zhao, T., Shi, J., Cosh, M.H., Chen, Y., Starks, P.J., Collins, C.H., Wu, S., Sun, R., Zheng, J., 2020. Global soil moisture retrievals from the Chinese FY-3D microwave radiation imager. IEEE Trans. Geosci. Remote Sens. 1–15. https://doi.org/10.1109/TGRS.2020.3019408.
Kawanishi, T., Sezai, T., Ito, Y., Imaoka, K., Takeshima, T., Ishido, Y., Shibata, A., Miura, M., Inahata, H., Spencer, R.W., 2003. The advanced microwave scanning radiometer for the earth observing system (AMSR-E), NASDA's contribution to the EOS for global energy and water cycle studies. IEEE Trans. Geosci. Remote Sens. 41, 184–193. https://doi.org/10.1109/TGRS.2002.808331.
Kerr, Y.H., Waldteufel, P., Wigneron, J.-P., Delwart, S., Cabot, F., Boutin, J., Escorihuela, M.-J., Font, J., Reul, N., Gruhier, C., Juglea, S.E., Drinkwater, M.R., Hahne, A., Martín-Neira, M., Mecklenburg, S., 2010. The SMOS Mission: new tool for monitoring key elements of the global water cycle. Proc. IEEE 98, 666–687. https://doi.org/10.1109/JPROC.2010.2043032.
Kerr, Y.H., Waldteufel, P., Richaume, P., Wigneron, J.P., Ferrazzoli, P., Mahmoodi, A., Al Bitar, A., Cabot, F., Gruhier, C., Juglea, S.E., Leroux, D., Mialon, A., Delwart, S., 2012. The SMOS soil moisture retrieval algorithm. IEEE Trans. Geosci. Remote Sens. 50, 1384–1403. https://doi.org/10.1109/TGRS.2012.2184548.
Kilic, L., Prigent, C., Aires, F., Boutin, J., Heygster, G., Tonboe, R.T., Roquet, H., Jimenez, C., Donlon, C., 2018. Expected performances of the Copernicus imaging microwave radiometer (CIMR) for an all-weather and high spatial resolution estimation of ocean and sea ice parameters. J. Geophys. Res. Ocean. 123, 7564–7580. https://doi.org/10.1029/2018JC014408.
Koike, T., Nakamura, Y., Kaihotsu, I., Davaa, G., Matsuura, N., Tamagawa, K., Fujii, H., 2004. Development of an advanced microwave scanning radiometer (Amsr-E) algorithm for soil moisture and vegetation water content. Proc. Hydraul. Eng. 48, 217–222. https://doi.org/10.2208/prohe.48.217.
Konings, A.G., McColl, K.A., Piles, M., Entekhabi, D., 2015. How many parameters can be maximally estimated from a set of measurements? IEEE Geosci. Remote Sens. Lett. 12, 1081–1085. https://doi.org/10.1109/LGRS.2014.2381641.
Konings, A.G., Piles, M., Rötzer, K., McColl, K.A., Chan, S.K., Entekhabi, D., 2016. Vegetation optical depth and scattering albedo retrieval using time series of dual-polarized L-band radiometer observations. Remote Sens. Environ. 172, 178–189. https://doi.org/10.1016/j.rse.2015.11.009.
Konings, A.G., Piles, M., Das, N., Entekhabi, D., 2017. L-band vegetation optical depth and effective scattering albedo estimation from SMAP. Remote Sens. Environ. 198, 460–470. https://doi.org/10.1016/j.rse.2017.06.037.
Lawrence, H., Wigneron, J.-P., Demontoux, F., Mialon, A., Kerr, Y.H., 2013. Evaluating the Semiempirical H–Q model used to calculate the L-band emissivity of a rough bare soil. IEEE Trans. Geosci. Remote Sens. 51, 4075–4084. https://doi.org/10.1109/TGRS.2012.2226995.
Li, Y., Shi, J., Liu, Q., Dou, Y., Zhang, T., 2015. The development of microwave vegetation indices from WindSat data. IEEE J. Sel. Top. Appl. Earth Obs. Remote Sens. 8, 4379–4395.
Meesters, A.G.C.A., De Jeu, R.A.M., Owe, M., 2005. Analytical derivation of the vegetation optical depth from the microwave polarization difference index. IEEE

Geosci. Remote Sens. Lett. 2, 121–123. https://doi.org/10.1109/LGRS.2005.843983.
Mialon, A., Richaume, P., Leroux, D., Bircher, S., Al Bitar, A., Pellarin, T., Wigneron, J.P., Kerr, Y.H., 2015. Comparison of Dobson and Mironov dielectric models in the SMOS soil moisture retrieval algorithm. IEEE Trans. Geosci. Remote Sens. 53 https://doi.org/10.1109/TGRS.2014.2368585.
Min, Q., Lin, B., 2006. Remote sensing of evapotranspiration and carbon uptake at Harvard Forest. Remote Sens. Environ. 100, 379–387. https://doi.org/10.1016/j.rse.2005.10.020.
Mironov, V.L., Dobson, M.C., Kaupp, V.H., Komarov, S.A., Kleshchenko, V.N., 2004. Generalized refractive mixing dielectric model for moist soils. IEEE Trans. Geosci. Remote Sens. 42, 773–785. https://doi.org/10.1109/TGRS.2003.823288.
Mo, T., Choudhury, B.J., Schmugge, T.J., Wang, J.R., Jackson, T.J., 1982. A model for microwave emission from vegetation-covered fields. J. Geophys. Res. Ocean 87, 11229–11237.
Njoku, E.G., Chan, S.K., 2006. Vegetation and surface roughness effects on AMSR-E land observations. Remote Sens. Environ. 100, 190–199. https://doi.org/10.1016/j.rse.2005.10.017.
Njoku, E.G., Li, L., 1999. Retrieval of land surface parameters using passive microwave measurements at 6-18 GHz. IEEE Trans. Geosci. Remote Sens. 37, 79–93. https://doi.org/10.1109/36.739125.
Njoku, E.G., Jackson, T.J., Lakshmi, V., Member, S., Chan, T.K., Nghiem, S.V., 2003. Soil Moisture Retrieval From AMSR-E. IEEE Trans. Geosci. Remote Sens. 41, 215–229.
O'Neill, P., Chan, S., Njoku, E., Jackson, T., Bindlish, R., 2018. Soil moisture active passive (SMAP) algorithm theoretical basis document: level 2 & 3 soil moisture (passive) data products. In: SMAP Project, JPL D-66480. Jet Propulsion Laboratory, Pasadena, CA.
O'Neill, P., Chan, S., Njoku, E., Jackson, T., Bindlish, R., 2019. SMAP Enhanced L3 Radiometer Global Daily 9 km EASE-Grid Soil Moisture, Version 3. NASA National Snow and Ice Data Center Distributed Active Archive Center, Boulder, Colorado USA. https://doi.org/10.5067/T90W6VRLCBHI.
Owe, M., De Jeu, R., Walker, J., 2001. A methodology for surface soil moisture and vegetation optical depth retrieval using the microwave polarization difference index. IEEE Trans. Geosci. Remote Sens. 39, 1643–1654. https://doi.org/10.1109/36.942542.
Owe, M., de Jeu, R., Holmes, T., 2008. Multisensor historical climatology of satellite-derived global land surface moisture. J. Geophys. Res. Earth Surf. 113, 1–17. https://doi.org/10.1029/2007JF000769.
Paloscia, S., Pampaloni, P., 1992. Microwave vegetation indexes for detecting biomass and water conditions of agricultural crops. Remote Sens. Environ. 40, 15–26. https://doi.org/10.1016/0034-4257(92)90123-2.
Paloscia, S., Macelloni, G., Santi, E., Koike, T., 2001. A multifrequency algorithm for the retrieval of soil moisture on a large scale using microwave data from SMMR and SSM/I satellites. IEEE Trans. Geosci. Remote Sens. 39 (8), 1655–1661.
Paloscia, S., Macelloni, G., Santi, E., 2006. Soil moisture estimates from AMSR-E brightness temperatures by using a dual-frequency algorithm. IEEE Trans. Geosci. Remote Sens. 44, 3135–3144.
Pampaloni, P., Paloscia, S., 1986. Microwave emission and plant water content: A comparison between field measurements and theory. IEEE Trans. Geosci. Remote Sens. GE-24, 900–905.
Parinussa, R.M., Holmes, T.R.H., De Jeu, R.A.M., 2012. Soil moisture retrievals from the windSat spaceborne polarimetric microwave radiometer. IEEE Trans. Geosci. Remote Sens. 50, 2683–2694. https://doi.org/10.1109/TGRS.2011.2174643.
Peng, B., Zhao, T., Shi, J., Lu, H., Mialon, A., Kerr, Y.H., Liang, X., Guan, K., 2017. Reappraisal of the roughness effect parameterization schemes for L-band radiometry over bare soil. Remote Sens. Environ. 199 https://doi.org/10.1016/j.rse.2017.07.006.
Rahmoune, R., Ferrazzoli, P., Member, S., Kerr, Y.H., Richaume, P., 2013. SMOS level 2 retrieval algorithm over forests: description and generation of global maps. IEEE J. Sel. Top. Appl. Earth Obs. Remote Sens. 6, 1430–1439. https://doi.org/10.1109/JSTARS.2013.2256339.
Rahmoune, R., Ferrazzoli, P., Singh, Y.K., Kerr, Y.H., Richaume, P., Al Bitar, A., 2014. SMOS retrieval results over forests: comparisons with independent measurements. IEEE J. Sel. Top. Appl. Earth Obs. Remote Sens. 7, 3858–3866. https://doi.org/10.1109/JSTARS.2014.2321027.
Robinson, D.A., Campbell, C.S., Hopmans, J.W., Hornbuckle, B.K., Jones, S.B., Knight, R., Ogden, F., Selker, J., Wendroth, O., 2008. Soil moisture measurement for ecological and hydrological watershed-scale observatories: a review. Vadose Zo. J. 7, 358. https://doi.org/10.2136/vzj2007.0143.
Rodríguez-Fernández, N.J., Mialon, A., Mermoz, S., Bouvet, A., Richaume, P., Al Bitar, A., Al-Yaari, A., Brandt, M., Kaminski, T., Le Toan, T., Kerr, Y.H., Wigneron, J.-P., 2018. An evaluation of SMOS L-band vegetation optical depth (L-VOD) data sets: high sensitivity of L-VOD to above-ground biomass in Africa. Biogeosciences 15, 4627–4645. https://doi.org/10.5194/bg-15-4627-2018.
Rodriguez-Fernandez, N.J., Mialon, A., Merlin, O., Suere, C., Cabot, F., Khazaal, A., Costeraste, J., Palacin, B., Rodriguez-Suquet, R., Tournier, T., Decoopman, T., Anterrieu, E., Colom, M., Morel, J.M., Kerr, Y.H., Rouge, B., Boutin, J., Picard, G., Pellarin, T., Escorihuela, M.J., Al Bitar, A., Richaume, P., 2019. SMOS-HR: a high resolution L-band passive radiometer for earth science and applications. Int. Geosci. Remote Sens. Symp. 8392–8395. https://doi.org/10.1109/IGARSS.2019.8897815.
Seneviratne, S.I., Corti, T., Davin, E.L., Hirschi, M., Jaeger, E.B., Lehner, I., Orlowsky, B., Teuling, A.J., 2010. Investigating soil moisture-climate interactions in a changing climate: a review. Earth Sci. Rev. 99, 125–161. https://doi.org/10.1016/j.earscirev.2010.02.004.
Shi, J., Jiang, L., Zhang, L., Chen, K.S., Wigneron, J.P., Chanzy, A., 2005. A parameterized multifrequency-polarization surface emission model. IEEE Trans. Geosci. Remote Sens. 43, 2831–2841. https://doi.org/10.1109/TGRS.2005.857902.
Shi, J., Jackson, T., Tao, J., Du, J., Bindlish, R., Lu, L., Chen, K.S., 2008. Microwave vegetation indices for short vegetation covers from satellite passive microwave sensor AMSR-E. Remote Sens. Environ. 112, 4285–4300. https://doi.org/10.1016/j.rse.2008.07.015.
Shi, J., Dong, X., Zhao, T., Du, J., Jiang, L., Du, Y., Liu, H., Wang, Z., Ji, D., Xiong, C., 2014. WCOM: the science scenario and objectives of a global water cycle observation mission. In: IEEE International Geoscience and Remote Sensing Symposium (IGARSS 2016), pp. 3646–3649.
Shi, J., Zhao, T., Cui, Q., Yao, P., 2019. Airborne and spaceborne passive microwave measurements of soil moisture. In: Li, X., Vereecken, H. (Eds.), Observation and Measurement of Ecohydrological Processes. Ecohydrology, vol 2. Springer, Berlin, Heidelberg. https://doi.org/10.1007/978-3-662-48297-1_3.
Talebiesfandarani, S., Zhao, T., Shi, J., Ferrazzoli, P., Wigneron, J.-P., Zamani, M., Pani, P., 2019. Microwave vegetation index from multi-angular observations and its application in vegetation properties retrieval: theoretical modelling. Remote Sens. 11 https://doi.org/10.3390/RS11060730.
Ulaby, F.T., Razani, M., Dobson, M.C., 1983. Effects of vegetation cover on the microwave radiometric sensitivity to soil moisture. IEEE Trans. Geosci. Remote Sens. GE-21, 51–61. https://doi.org/10.1109/TGRS.1983.350530.
Van De Griend, A.A., Wigneron, J.P., 2004. On the measurement of microwave vegetation properties: some guidelines for a protocol. IEEE Trans. Geosci. Remote Sens. 42, 2277–2289. https://doi.org/10.1109/TGRS.2004.832243.
Vereecken, H., Huisman, J.A., Bogena, H., Vanderborght, J., Vrugt, J.A., Hopmans, J.W., 2008. On the value of soil moisture measurements in vadose zone hydrology: a review. Water Resour. Res. 46, 1–21. https://doi.org/10.1029/2008WR006829.
Vittucci, C., Vaglio Laurin, G., Tramontana, G., Ferrazzoli, P., Guerriero, L., Papale, D., 2019. Vegetation optical depth at L-band and above ground biomass in the tropical range: evaluating their relationships at continental and regional scales. Int. J. Appl. Earth Obs. Geoinf. 77, 151–161. https://doi.org/10.1016/j.jag.2019.01.006.
Wang, J.R., Choudhury, B.J., 1981. Remote sensing of soil moisture content over bare fields at 1.4 GHz frequency. J. Geophys. Res. 86, 5277–5282.
Watanabe, S., 1960. Information theoretical analysis of multivariate correlation. IBM J. Res. Dev. 4, 66–82. https://doi.org/10.1147/rd.41.0066.
Wigneron, J.P., Chanzy, A., Calvet, J.C., Bruguier, N., 1995a. A simple algorithm to retrieve soil moisture and vegetation biomass using passive microwave measurements over crop fields. Remote Sens. Environ. 51, 331–341. https://doi.org/10.1016/0034-4257(94)00081-W.
Wigneron, J.-P., Laguerre, L., Kerr, Y.H., 2001. A simple parameterization of the L-band microwave emission from rough agricultural soils. IEEE Trans. Geosci. Remote Sens. 39, 1697–1707. https://doi.org/10.1109/36.942548.
Wigneron, J.P., Calvet, J.C., Pellarin, T., Van De Griend, A.A., Berger, M., Ferrazzoli, P., 2003. Retrieving near-surface soil moisture from microwave radiometric observations: current status and future plans. Remote Sens. Environ. 85, 489–506. https://doi.org/10.1016/S0034-4257(03)00051-8.
Wigneron, J.P., Member, S., Pardé, M., Waldteufel, P., Chanzy, A., Kerr, Y., Member, S., Schmidl, S., Skou, N., 2004. Characterizing the dependence of vegetation model parameters on crop structure. Incidence Angle Polar. L Band 42, 416–425.
Wigneron, J.P., Kerr, Y., Waldteufel, P., Saleh, K., Escorihuela, M.J., Richaume, P., Ferrazzoli, P., de Rosnay, P., Gurney, R., Calvet, J.C., Grant, J.P., Guglielmetti, M., Hornbuckle, B., Mätzler, C., Pellarin, T., Schwank, M., 2007. L-band microwave emission of the biosphere (L-MEB) model: description and calibration against experimental data sets over crop fields. Remote Sens. Environ. 107, 639–655. https://doi.org/10.1016/j.rse.2006.10.014.
Wigneron, J.P., Chanzy, A., De Rosnay, P., Rüdiger, C., Calvet, J.C., 2008. Estimating the effective soil temperature at L-band as a function of soil properties. IEEE Trans. Geosci. Remote Sens. 46, 797–807. https://doi.org/10.1109/TGRS.2007.914806.
Wigneron, J.P., Chanzy, A., Kerr, Y.H., Lawrence, H., Shi, J., Escorihuela, M.J., Mironov, V., Mialon, A., Demontoux, F., De Rosnay, P., Saleh-Contell, K., 2011. Evaluating an improved parameterization of the soil emission in L-MEB. IEEE Trans. Geosci. Remote Sens. 49, 1177–1189.
Wigneron, J.P., Jackson, T.J., O'Neill, P., De Lannoy, G., de Rosnay, P., Walker, J.P., Ferrazzoli, P., Mironov, V., Bircher, S., Grant, J.P., Kurum, M., Schwank, M., Munoz-Sabater, J., Das, N., Royer, A., Al-Yaari, A., Al Bitar, A., Fernandez-Moran, R., Lawrence, H., Mialon, A., Parrens, M., Richaume, P., Delwart, S., Kerr, Y., 2017. Modelling the passive microwave signature from land surfaces: A review of recent results and application to the L-band SMOS & SMAP soil moisture retrieval algorithms. Remote Sens. Environ. https://doi.org/10.1016/j.rse.2017.01.024.
Zhao, T.J., Zhang, L.X., Shi, J.C., Jiang, L.M., 2011. A physically based statistical methodology for surface soil moisture retrieval in the Tibet plateau using microwave vegetation indices. J. Geophys. Res. 116, D08116 https://doi.org/10.1029/2010jd015229.
Zhao, T., Shi, J., Lin, M., Yin, X., Liu, Y., Lan, H., Xiong, C., 2014. Potential soil moisture product from the Chinese HY-2 scanning microwave radiometer and its initial assessment. J. Appl. Remote. Sens. 8, 083560 https://doi.org/10.1117/1.jrs.8.083560.
Zhao, T., Shi, J., Bindlish, R., Jackson, T., Cosh, M., Jiang, L., Zhang, Z., Lan, H., 2015a. Parametric exponentially correlated surface emission model for L-band passive microwave soil moisture retrieval. Phys. Chem. Earth 83–84, 65–74.
Zhao, T., Shi, J., Bindlish, R., Jackson, T.J., Kerr, Y.H., Cosh, M.H., Cui, Q., Li, Y., Xiong, C., Che, T., 2015b. Refinement of SMOS multiangular brightness temperature toward soil moisture retrieval and its analysis over reference targets. IEEE J. Sel.

Top. Appl. Earth Obs. Remote Sens. 8, 589–603. https://doi.org/10.1109/JSTARS.2014.2336664.

Zhao, T., Shi, J., Lv, L., Xu, H., Chen, D., Cui, Q., Jackson, T.J., Yan, G., Jia, L., Chen, L., Zhao, K., Zheng, X., Zhao, L., Zheng, C., Ji, D., Xiong, C., Wang, T., Li, R., Pan, J., Wen, J., Yu, C., Zheng, Y., Jiang, L., Chai, L., Lu, H., Yao, P., Ma, J., Lv, H., Wu, J., Zhao, W., Yang, N., Guo, P., Li, Y., Hu, L., Geng, D., Zhang, Z., 2020a. Soil moisture experiment in the Luan River supporting new satellite mission opportunities. Remote Sens. Environ. 240, 111680. https://doi.org/10.1016/j.rse.2020.111680.

Zhao, T., Hu, L., Shi, J., Lü, H., Li, S., Fan, D., Wang, P., Geng, D., Kang, C.S., Zhang, Z., 2020b. Soil moisture retrievals using L-band radiometry from variable angular ground-based and airborne observations. Remote Sens. Environ. 248, 111958. https://doi.org/10.1016/j.rse.2020.111958.